Master in Chemical Engineering

Advanced Modelling of PSA Processes for Biogas Upgrading

Master Thesis

Mónica Patrícia da Silva Santos

Supervisor: **Prof. Alírio Rodrigues**

Co-Supervisor: **Dr. Carlos Grande**

U.PORTO
FEUP FACULDADE DE ENGENHARIA
UNIVERSIDADE DO PORTO

LSRE – Laboratory of Separation and Reaction Engineering

Department of Chemical Engineering

Faculty of Engineering

University of Porto

July 2011

Aos meus pais….

Acknowledgments

Nesta secção quero agradecer a todos aqueles que de um modo ou de outro contribuíram para a realização desta tese.

Gostaria de agradecer aos meus orientadores, Professor Alírio Rodrigues e Dr. Carlos Grande. Ao Prof. Alírio pela disponibilidade demonstrada e ao Dr. Carlos Grande, que mesmo à distância, apoiou a execução desta tese e sempre se disponibilizou para me esclarecer.

Quero também agradecer a todos os colegas e amigos do LSRE.

Aos meus pais, “os meus pilares”, pela sua constante presença em todos os momentos da minha vida. Um muito obrigado.

Por fim, quero agradecer ao Carlos Eduardo, pelo seu apoio, incentivo e sentido crítico.

Abstract

This work focused on the application of Pressure Swing Adsorption (PSA) for the upgrading of biogas to obtain bio-methane (purity > 98%) that can be used as renewable fuel. The effect of operating conditions using different materials (zeolite 13X and carbon molecular sieve 3K) was studied. Due to the high steepness of CO_2 adsorption on zeolite 13X it was observed that increasing the temperature from ambient to 323 K it is possible to improve the performance of the PSA unit and obtain bio-methane with purity higher than 99 % , recovery of 85 % and power consumption of 0.12 $kW \cdot mol^{-1}$ of produced methane.

Instead of the classical single-column simulation to describe the PSA performance, the more realistic multi-column PSA cycle was also investigated. A comparison of the results obtained between simulations using one-column simulation and two-column simulation was carried out to determine the effect of recycling contaminated streams in purge and pressure equalization steps. The results were obtained with a two-column PSA process using six-step cycle compressing pressurization, feed, depressurization, blowdown, purge and pressure equalization. It was found that the recycle of streams with purity lower than 99 % results in a significant decrease in the overall purity of bio-methane.

Finally, a new multi-column cycle was proposed with special emphasis in improving the PSA performance when using kinetic adsorbents. These adsorbents, carbon molecular sieves for example, are characterized by having slow adsorption kinetics resulting in large mass transfer zone (MTZ) inside the column. In this new column arrangement, when the heavy (most adsorbed) gas breaks through one column, the exit of this column is connected to other column (trim bed) where more heavy gas can be adsorbed. In this way, also more heavy gas will be adsorbed in the first (lead) column. The increase of process performance is directly related to the length of the MTZ: the larger the MTZ, the better will perform using the lead-trim beds concept. Two different adsorbents were employed in the process simulations: zeolite 13X (fast diffusion) and carbon molecular sieve (slow diffusion). Using this new cycle, it was possible to obtain high purity bio-methane and unit productivity of 5.5 mol CH_4 per hour per kilogram of carbon molecular sieve.

Keywords: adsorption, biogas, zeolite 13X, carbon molecular sieve 3K, Pressure Swing Adsorption

Resumo

Este trabalho focou-se sobre a aplicação da Adsorção com Modulação de Pressão (AMP) na purificação do biogás para obter biometano (> grau de pureza; 98 %), sendo este gás considerado uma fonte renovável de energia que pode ser usado como combustível. Foi estudado o efeito das condições de operação empregando diferentes materiais (zeólito 13X e peneira molecular de carbono 3K). Devido ao declive acentuado da isotérmica de adsorção do CO_2 no zeólito 13X observou-se que aumentando a temperatura de operação para 323 K é possível melhorar o desempenho da unidade de AMP. Foi possível obter biometano com uma pureza superior a 99 %, com uma recuperação de 85 % e um consumo energético de 0.12 $kW \cdot mol^{-1}$ de metano produzido.

Em vez da simulação clássica de uma coluna para descrever o desempenho da unidade de AMP, a fim de se aproximar à prática real, foi estudado o desempenho de um ciclo com várias colunas de AMP. Os resultados obtidos nas simulações para uma e duas colunas foram comparados para determinar o efeito de reciclo de correntes contaminadas nas etapas de purga e de equalização de pressão. Os resultados foram obtidos para um processo de AMP com duas colunas usando um ciclo com seis etapas: pressurização, produção, despressurização intermédia, despressurização, purga e equalização de pressão. Observou-se que o reciclo de correntes com uma pureza inferior a 99 % conduz a uma diminuição significativa na pureza total do biometano.

Finalmente, um novo ciclo com várias colunas foi proposto para melhorar, com especial ênfase, o desempenho da AMP empregando adsorventes cinéticos. Estes adsorventes, por exemplo as peneiras moleculares de carbono, são caracterizados por uma cinética lenta de adsorção tendo por resultado uma grande zona de transferência massa (ZTM) dentro da coluna. Neste novo arranjo de coluna, quando o gás pesado (o mais adsorvido) rompe à saída da coluna, a saída desta é conectada a uma outra (“trim bed”) onde mais gás pesado pode ser adsorvido. Deste modo, mais gás pesado será adsorvido igualmente na primeira coluna (“lead bed”). O aumento do desempenho do processo é relacionado directamente com o comprimento da ZTM: quanto maior a ZTM, melhor será o desempenho do conceito “lead-trim beds”. Dois adsorventes diferentes foram empregues nas simulações do processo: zeólito 13X (difusão rápida) e peneira molecular de carbono (difusão lenta). Usando este novo ciclo, foi possível obter biometano com um elevado grau de pureza e uma produtividade de 5.5 mol de CH_4 por hora e por quilograma de peneira molecular de carbono.

Contents

Acknowledgments i

Abstract ii

Resumo iii

Contents i

List of Figures ii

List of Tables iv

Notation vi

1. Introduction 1

1.1. Motivation and Relevance 1

1.2. Objectives and Outline 3

2. State of the Art 5

2.1. Biogas 5

2.2. Pressure Swing Adsorption (PSA) 5

3. Fundamental Concepts of Adsorption 7

3.1. The Adsorbent 7

3.1.1. Zeolites 8

3.1.2. Carbon Molecular Sieves (CMS) 9

3.2. Models for the Description of the Gas Adsorption Equilibrium 9

3.2.1. The Langmuir Model 9

3.2.2. The Freundlich Model 10

3.2.3. The Toth Model 10

3.2.4. The Multi-Site Langmuir or Nitta Model 11

3.3. Adsorption kinetics. Diffusion in Porous Media 12

3.3.1. Molecular Diffusion 12

3.3.2. Knudsen Diffusion 13

3.3.3. Poiseuille Flow 14

4. Modelling of Pressure Swing Adsorption 16

4.1. Adsorption equilibrium and kinetics 16

4.2. Mathematical modelling of fixed-bed column 17

4.3. Modified Skarstrom cycle and performance variables 20

5. Simulation of a PSA Process for Biogas Upgrading 24

5.1. PSA sizing 24

5.2. Simulation of 1-column PSA 26

5.3. Effect of recycling streams in PSA 28

6. New Cycle Configuration to Enhance Performance of Kinetic PSA Processes 32

6.1. Cycle design 32

6.2. Results and Discussion 34

6.2.1. Cycle I: 9-step lead-trim operation 36

7. Conclusions and Recommendation for Future Work 42

7.1. Conclusions 42

7.2. Objectives Achieved and Recommendation for Future Work 43

References 44

Appendix 51

A. Correlations used for estimation of mass and heat transfer parameters employed in the mathematic model 51

B. Boundary and initial conditions of the PSA model 52

C. Preliminary Studies: 1-Column PSA performance 54

D. Cycle II: 11-step higher pressure purge step 56

List of Figures

Figure 3.1. Activated Carbon adsorbs gases and chemicals. 7

Figure 3.2. Mechanisms of diffusion on macropore: a) Molecular Diffusion; b) Knudsen Diffusion; c) Poiseuille Diffusion. 14

Figure 4.1. Adsorption equilibrium isotherms on zeolite 13X of (a) CO_2 and (b) CH_4 16

Figure 4.2. PSA cycle scheme (a) and pressure history of one CSS cycle (b) for a six steps 1-column PSA simulation.....21

Figure 4.3. PSA cycle scheme (a) and pressure history of one CSS cycle (b) for a six steps 2-column PSA simulation.....22

Figure 5.1(a) Molar flowrate of CH_4 and CO_2 and (b) temperature profiles at 0.3, 0.8 and 1.25 m from feed inlet for a simulated binary curve (67 % of CH_4 balanced by CO_2) at 323 K, 4 bar with a total feed flowrate of 347.2 SLPM. 25

Figure 5.2. 1-column simulation of PSA for CH_4-CO_2 separation using zeolite 13X. Cycle scheme is shown in Figure 4.2 and operating conditions in Table 5.3 (Run 21). Results presented are: a) Molar flowrate of each gas exiting the column, b) temperature histories at different positions (0.3, 0.6, 1 and 1.25 m) from feed inlet, for cyclic steady state, amount adsorbed of c) CO_2 and d) CH_4. 27

Figure 5.3. 2-column simulation of PSA for CH_4-CO_2 separation using zeolite 13X. Cycle scheme is shown in Figure 4.3 and operating conditions in Table 5.4 (Run d, 2 bed). Results presented are: a) Molar flowrate of each gas exiting the column, b) temperature histories at different positions (0.3, 0.6, 1 and 1.25 m) from feed inlet, for cyclic steady state, amount adsorbed of c) CO_2 and d) CH_4. 30

Figure 5.4. Simulation results for PSA cycle employing one and two columns with cycle scheme showed in Figures 4.2 and 4.3, respectively.. 31

Figure 6.1. PSA cycle scheme used in simulation for PSA Cycle I.....33

Figure 6.2. 4-column simulation of PSA for CH_4-CO_2 separation using CMS-3K. Cycle scheme is shown in Figure 6.1 and operating conditions in Table 6.2 (Run i). Results presented are: a) molar flowrate of each gas exiting the column and b) and typical pressure history of one CSS cycle used in simulation for PSA Cycle I.. 37

Figure 6.3. 4-column simulation of PSA for CH_4-CO_2 separation using CMS-3K. Cycle scheme is shown in Figure 6.1 and operating conditions in Table 6.2 (Run i). Results presented are: a) gas phase concentration of CO_2, b) amount adsorbed of CO_2, c) amount adsorbed of CH_4 and d) steady state temperature profiles at different positions (0.3, 0.6, 1 and 1.25 m) from feed inlet..38

Figure 6.4. 4-column simulation of PSA for CH_4-CO_2 separation using Zeolite 13X. Cycle scheme is shown in Figure 6.1 and operating conditions in Table 6.3 (Run e). Results presented are: a) molar flowrate of each gas exiting the column and b) steady state temperature profiles at different positions (0.3, 0.6, 1 and 1.25 m) from feed inlet. 40

Figure 6.5. 4-column simulation of PSA for CH_4-CO_2 separation using Zeolite 13X. Cycle scheme is shown in Figure 6.1 and operating conditions in Table 6.3 (Run e). Results presented are: a) gas phase concentration of CO_2, b) amount adsorbed of CO_2 and c) amount adsorbed of CH_4. 41

Figure C.1. Effect of purge flowrate in 1-column PSA performance: (a) CH_4 purity and recovery and (b) unit productivity and power consumption. 55

Figure C.2. Effect of purge time in 1-column PSA performance: (a) CH_4 purity and recovery and (b) unit productivity and power consumption. 55

Figure D.1. PSA cycle scheme used in simulation for PSA Cycle II.. 56

Figure D.2. 4-column simulation of PSA for CH_4-CO_2 separation using CMS-3K. Cycle scheme is shown in Figure D.1 and operating conditions in Table D.1. (Run n). Results presented are: a) molar flowrate of each gas exiting the column and b) and typical pressure history of one CSS cycle used in simulation for PSA Cycle II.. 57

List of Tables

Table 3.1. Characteristic of major synthetic zeolite adsorbents. 8

Table 4.1. Adsorption equilibrium and kinetic parameters of CH_4 and CO_2 adsorption on zeolite 13X and CMS-3K. 17

Table 5.1. Physical properties of zeolite 13X used in the breakthrough and PSA simulations. ... 24

Table 5.2. Column characteristics and operating conditions used in the breakthrough and PSA simulations. 25

Table 5.3. 1-Column PSA performance for CH_4/CO_2 separation using zeolite 13X with modified Skarstrom cycle. 26

Table 5.4. Comparison between the predicted performance of the studied PSA employing 1-column and 2-columns simulations. 29

Table 6.1. Physical properties of the CMS-3K employed in the PSA simulations. 35

Table 6.2. 4-Column PSA performance for CH_4/CO_2 separation using CMS-3K and the first cycle configuration. 39

Table 6.3. 4-Column PSA performance for CH_4/CO_2 separation using Zeolite 13X and the first cycle configuration. 40

Table A.1. Correlations used for estimation of mass and heat transfer parameters 51

Table B.1. Boundary and initial conditions of a PSA process for CO_2/CH_4 separation 52

Table C.1. 1-Column PSA performance for CH_4/CO_2 separation using zeolite 13X with modified Skarstrom cycle.. 54

Table D.1. 4-Column PSA performance for CH_4/CO_2 separation using CMS-3K and the second cycle configuration. 58

Table D.2. 4-Column PSA performance for CH_4/CO_2 separation using zeolite 13X and the second cycle configuration. 58

Notation

a_i	number of neighbouring sites occupied by component i
a_p	particle specific area (m^{-1})
A_i	parameters relating the thermal variation of the heterogeneity coefficient
$\dot{B}$	molar flowrate to be compressed
B_i	parameters relating the thermal variation of the heterogeneity coefficient
Bi_i	mass Biot number of component i
C_i	gas phase concentration of component i ($mol \cdot m^{-3}$)
$\tilde{\tilde{C}}_p$	molar constant pressure specific heat of the gas mixture ($J \cdot mol^{-1} \cdot K^{-1}$)
$\tilde{\tilde{C}}_{p_s}$	constant volumetric specific heat of component i ($J \cdot kg^{-1} \cdot K^{-1}$)
$\langle C_{p,i} \rangle$	macropore averaged concentration of component i ($mol \cdot m^{-3}$)
$\tilde{\tilde{C}}_{pw}$	constant pressure specific heat of the column wall ($J \cdot kg^{-1} \cdot K^{-1}$)
$\tilde{\tilde{C}}_{vi}$	molar constant volumetric specific heat of component i ($J \cdot mol^{-1} \cdot K^{-1}$)
$\tilde{\tilde{C}}_{v,ads,i}$	molar constant volumetric specific heat of component i adsorbed ($J \cdot mol^{-1} \cdot K^{-1}$)
d_p	particle diameter (m)
d_{wi}	wall internal diameter (m)
D	column diameter (m)
D_{ax}	axial dispersion coefficient ($m^2 \cdot s^{-1}$)
$D_{k,i}$	Knudsen diffusivity of component i ($m^2 \cdot s^{-1}$)
$D_{m,i}$	molecular diffusivity of component i ($m^2 \cdot s^{-1}$)
$D_{p,i}$	macropore diffusivity of component i ($m^2 \cdot s^{-1}$)
$D_{u,i}^{\infty}$	micropore diffusivity of component i at infinite dilution ($m^2 \cdot s^{-1}$)
$D_{u,i}^{0}$	diffusivity of component i at infinite temperature ($m^2 \cdot s^{-1}$)
e	wall thickness (m)
Ea_i	activation energy of micropore diffusion of component i ($J \cdot mol^{-1}$)
F_{CH_4}	number of CH_4 moles fed to the column in pressurization and feed steps (mol)
h_f	film heat transfer coefficient between the gas and the solid phase ($W \cdot m^{-2} \cdot K^{-1}$)
h_w	wall heat transfer coefficient between the gas and the column wall ($W \cdot m^{-2} \cdot K^{-1}$)
J	diffusion flux ($mol \cdot m^{-1} \cdot s^{-1}$)
k	Boltzmann constant ($m^2 \cdot kg \cdot s^{-2} \cdot K^{-1}$)
k_{blow}	constant for describing the time-evolution of variables and fluxes at boundaries, in the

	blowdown step (s^{-1})
k_{blow_eq}	constant for describing the time-evolution of variables and fluxes at boundaries, in the pressure equalization depressurization step (s^{-1})
k_f	film mass transfer coefficient ($m \cdot s^{-1}$)
k_g	gas thermal conductivity ($W \cdot m^{-1} \cdot K^{-1}$)
$K_{b,i}$	barrier mass transfer coefficient of component i ($m^2 \cdot s^{-1}$)
K_i	equilibrium constant of component i in the multisite Langmuir isotherm (Pa^{-1})
K_i^0	equilibrium constant at the limit $T \to \infty$ of component i (Pa^{-1})
$K_{u,i}$	micropore diffusivity of component i ($m^2 \cdot s^{-1}$)
$K_{u,i}^0$	limiting diffusivity at infinite temperature of component i ($m^2 \cdot s^{-1}$)
L	column length (m)
M_w	molecular weight ($kg \cdot mol^{-1}$)
n_i	adsorbent heterogeneity
Nu	Nusselt number
P	pressure (bar)
n_i	adsorbent heterogeneity
$\dot{n}_{feed}$	moles of biogas available per unit of time ($mol \cdot s^{-1}$)
N_{CH_4}	number of CH_4 moles exiting the column in feed step (mol)
N_{CO_2}	number of CO_2 moles exiting the column in feed step (mol)
P_{low}	blowdown pressure (bar)
P_E	equalization pressure (bar)
P_{high}	discharge pressure (bar)
Pr	Prandtl number
$q_{i,max}$	maximum adsorbed phase concentration of component i ($mol \cdot kg^{-1}$)
$\langle \bar{q}_i \rangle$	macropore averaged adsorbed phase concentration of component i ($mol \cdot kg^{-1}$)
q_i^*	adsorbed phase in equilibrium with the average concentration in the macropores ($mol \cdot kg^{-1}$)
Q_{feed}	feed flowrate (SLPM)
Q_{purge}	purge flowrate (SLPM)
r_p	pore radius (m)
R_{CH_4}	number of CH_4 moles used in pressurization and purge steps (mol)
Re	Reynolds number
R_g	universal gas constant ($J \cdot mol^{-1} \cdot K^{-1}$)

R_p	particle radius (m)
R_w	radius of the column wall (m)
Sc	Schmidt number
Sh	Sherwood number
t	time (s)
t_{blow}	blowdown step time (s)
t_{feed}	feed step time (s)
t_{lead}	feed 2 and lead adsorption steps times (s)
t_{press}	pressurization step time (s)
t_{trim}	trim feed step time (s)
t_{purge}	purge step time (s)
T_{feed}	feed temperature (K)
T_g	gas temperature (K)
T_s	solid phase temperature (K)
T_w	column wall temperature (K)
T_∞	ambient temperature (K)
u_0	superficial velocity ($m \cdot s^{-1}$)
U	global external heat transfer coefficient ($W \cdot m^{-2} \cdot K^{-1}$)
x	coordinate (m)
$y_{CH4,feed}$	molar fraction of methane in the feed and lead steps
y_i	molar fraction of component i
z	axial position (m)

Greek letters

α_w	ratio of the internal surface area to the volume of the column wall (m^{-1})
α_{wl}	ratio of the logarithmic mean surface area of the column shell to the volume of the column wall (m^{-1})
ϵ	attractive force constant in Lennard-Jones potential
ε_c	bed porosity
ε_p	particle porosity
γ	equal to 3/2 for ideal gases
λ	heat axial dispersion coefficient ($W \cdot m^{-2} \cdot K^{-1}$)
$\Delta H_{ads,i}$	heat of adsorption of component i ($J \cdot mol^{-1}$)
η	mechanical efficiency (assumes a value of 0.8)

μ	gas viscosity (Pa·s)
ρ_b	bulk density (kg·m^{-3})
ρ_g	gas density (kg·m^{-3})
ρ_p	particle density (kg·m^{-3})
ρ_w	column wall density (kg·m^{-3})
τ_p	pore tortuosity
σ_{12}	collision diameter from the Lennard-Jones potential (A)
Ω	function of ϵ/kT

1. Introduction

1.1. Motivation and Relevance

There are several studies of CH_4 / CO_2 separation, where the separation was performed with adsorbents that allow operation under kinetic-control regime (Cavenati, et al, 2005; Delgado et al., 2006a; Delgado et al., 2007; Gomes and Hassan, 2001; Grande and Rodrigues, 2007a; Kapoor and Yang, 1989; Kim et al., 2006; Pilarczyk et al., 1988; Schroter et al., 1989; Yang, 1987). However, there are also few studies, for the same mixture, operating with equilibrium adsorbents (Bonnot and Tondeur, 2006; Delgado et al., 2006b; Grande and Rodrigues, 2007a, b). Four (Skarstrom cycle, Skarstrom, 1960) or five steps single bed were considered in those studies. It was previously demonstrated that kinetic-based adsorbents may result in higher overall productivities than equilibrium-based adsorbents (Grande and Rodrigues, 2007a). The main reason for that was the strong non-linearity of the isotherms of equilibrium-based adsorbents like zeolites (Yang, 1987). However, the performance of equilibrium-based materials can be improved if higher temperatures are employed.

One objective of this work is to demonstrate that equilibrium-based adsorbents can significantly contribute to bio-methane production from thermophilic digestors where temperature is around 323 K (Zupancˇicˇ and Rosˇ, 2003). The feed conditions, corresponding to the biogas from thermofilic digestors, were fixed: 500 $m^3 \cdot day^{-1}$ (measured in standard conditions, 296.15 K and 1 atm), available at 323 K and with 67 % of CH_4 and 33 % CO_2. The flowrate of 500 $m^3 \cdot day^{-1}$ with such composition can be obtained in waste-water treatment plants and in small/medium biogas digesters using crop residues. Several Pressure Swing Adsorption (PSA) simulations were performed to obtain a product (CH_4) with over 98 % of purity and high recovery. The influence of multi-column operation was studied using a modified Skarstrom cycle comprising: co-current pressurization with feed, feed, co-current pressure equalization depressurization, counter-current blowdown, counter-current purge with product and counter-current pressure equalization pressurization. The introduction of an equalization step introduced a great improvement in the PSA process (Berlin, 1966; Delgado and Rodrigues, 2008; Marsh et al., 1964; Wagner, 1969; Warmuzinski, 2002). The design of a PSA can be done by studying the performance of one column and avoiding recycling of gases from other columns. So far all biogas separation work in Laboratory of Separation and Reaction Engineering (LSRE) (Cavenati, et al, 2005; Grande and Rodrigues, 2007a, b) were performed employing only one column where the purge step was performed with pure methane. However, in industrial

processes, where a multicolumn system is employed, and a stream with 0.1 % up to 2 % of CO_2 is recycled in the pressure equalization(s) and purge steps, the result is a higher contamination of the product stream. For that reason to obtain more realistic results, the performance of all the columns and the impurities present in the recycled streams should be taken into account. The effect of recycling dirty streams was evaluated since the objective is to produce methane with 98 % purity (contamination of CO_2 may reach 2 %). However, the design of a PSA unit using kinetic adsorbents is challenging because the design cannot be performed using the simplified equilibrium theory concept (LeVan, 1998; Ruthven et al., 1994). In fact, using the equilibrium theory, one assumption is that the diffusion is very fast and thus the mass transfer zone (MTZ) happens in a small portion of the column. However, PSA process using adsorbents with slow diffusion kinetics are known by having large MTZ, often larger than the column length (Keller et al., 1987). Due to the large MTZ, the effective adsorption loading attained in each column is far distant from the maximum (equilibrium) adsorption loading. A direct consequence of this sub-utilization of the columns is a low productivity of kinetic PSA processes.

Any improvement of the process performance will reduce the size and thus the initial investment of the separation. It was previously suggested that connecting two beds in series (lead-trim) can be advantageous since there is more contact time between the gas and the adsorbent (Keller et al., 1987). This concept was initially developed for TSA processes where the column regeneration is performed at higher temperature than adsorption. The adsorbent temperature should be increased to promote desorption almost always followed by a purge to remove the desorbed gas. After that, a cooling step should be done to return the column to adsorption condition (Keller et al., 1987). If this step begins only after all the heated bed, the adsorption column will remain at that temperature for the time that the cooling front takes to cross it and consequently, much of the heat is removed from the bed. One way to overcome this limitation is putting the beds in series; one bed is on adsorption, other on regeneration and a third on cooling step. The MTZ passes completely through the first (lead) column into the second (trim) bed. After the lead bed is saturated it should be regenerated and the trim bed becomes the lead bed. In order to carry out this separation, a minimum of three columns should be employed. Although this concept was described for Temperature Swing Adsorption (TSA) operation dealing with diluted mixtures, it is possible to extend this concept to PSA processes.

In this work, this lead-trim concept is employed for the operation of a new PSA cycle, specially focused for kinetic adsorbents. We have taken as example the removal carbon dioxide of from biogas (33 % CO_2 and 67 % CH_4) with the aim of obtaining methane with purity higher than 98 % (Cavenati et al., 2005; Hagen et al., 2001; Knaebel and Reynhold, 2002; Petersson and

Wellinger, 2009). Simulations of the PSA cycle using two different adsorbents was carried out. The first adsorbent is zeolite 13X where the diffusion is very fast and the long mass transfer zone is caused by thermal effects while the second adsorbent is carbon molecular sieve 3K (CMS-3K) where diffusion of methane is extremely slow. The possibility of reducing power consumption by performing purge at higher pressure was also analyzed.

1.2. Objectives and Outline

The general objective of this thesis is the upgrading of biogas by Pressure Swing Adsorption (PSA). The first part is dedicated to study the recycle effect of highly contaminated streams in the PSA performance, particularly in the methane purity. For this purpose, several simulations of a process for binary separation of CH_4-CO_2 using zeolite 13X as selective adsorbent were carried out at 323 K. This temperature was chosen after a preliminary study and by comparison with previous works already performed, in LSRE, for this separation on this adsorbent. The results obtained with a two-column PSA process using six-step cycle (pressurization, feed, depressurization, blowdown, purge and pressure equalization) were compared with those attained by simulating the behaviour of only one column. The objective of the second part was to study a new PSA cycle to improve the utilization of the kinetic adsorbent in multi-column PSA processes.

This thesis begins, in Chapter 1, with a short description of the work, presenting the relevance and motivation and the objectives.

The climate is changing due the accumulation of greenhouses gases (GHG) in the atmosphere which contributes to the Global Warming. CO_2 and CH_4 are the major greenhouse gases from human sources, being the greenhouse warming potential (GWP) of methane 21 times higher than for CO_2. In Chapter 2 the major sources of biogas and the technologies to separate it are presented, with special emphasis for the pressure swing adsorption process.

A brief description of the adsorbents employed in this thesis is given in Chapter 3: zeolite 13X and carbon molecular sieve 3K. The main adsorption equilibrium models, Langmuir, Freundlich, Toth and Multi-Site Langmuir, are also described as well as the diffusion kinetics in the adsorbent particles (molecular diffusion, Knudsen diffusion, Poiseuille flow, micropore diffusion and pore mouth resistance of micropores). The mathematic model of a PSA process is described in Chapter 4. The adsorption equilibrium and kinetics of CO_2 and CH_4 on zeolite 13X and CMS-3K are also shown in this Chapter, as well as the configuration of a modified Skarstrom cycle and it performance variables.

Most of the research work published for biogas separation was performed with kinetic adsorbents and few works were carried out with equilibrium adsorbents, in this case, the zeolite 13X. For this purpose and to improve the biogas separation employing zeolite 13X as adsorbent, in the Chapter 5 several simulations were performed and a Skarstrom modified cycle was studied for one and two column PSA process. The increase of temperature to 323 K was also studied.

PSA processes that employ kinetic adsorbents, with slow diffusion kinetics, lead to a large mass transfer zone (MTZ). For this reason, the effective adsorption loading decreases which results in a low productivity of processes. In Chapter 6 it is proposed an alternative to modify the properties of the bed without changing the properties of the adsorbent. Therefore, a new cycle configuration was proposed to enhance the PSA performance employing this adsorbent type. The carbon molecular sieve 3K was the kinetic adsorbent chosen.

Chapter 7 presents the conclusions of this work and the suggestions for future work.

2. State of the Art

2.1. Biogas

Methane (CH_4), like carbon dioxide (CO_2) gas, is a significant contributor to the accumulation of greenhouse gases (GHG) and consequently for increased global warming (Pritchard, 2004): the greenhouse warming potential (GWP) of methane is 21 times higher than for CO_2 (Knaebel and Reynhold, 2002). Principal sources of methane emissions to atmosphere are: natural gas systems, enteric fermentation, landfills and wastewater treatment plants. Tighter control in methane emissions will have a significant contribution in mitigating anthropogenic emissions. Landfill gas (LFG) and the biogas generated in anaerobic digestion units of wastewater treatment plants (WWTPs) are the main sources of methane emissions in several countries (GHG Data). Considering that this methane can also be used for energy or fuel production, this is a win-win situation for the generation of a bio-fuel. For this reason, it is the bio-fuel with higher tons of CO_2 avoided (FBAE).

The use of bio-methane as fuel or its injection in a pipeline for grid distribution, introduces some quality specifications for biogas. Despite of the removal of several contaminants (siloxanes, H_2S), the gas should have a very small content of water and carbon dioxide concentration below 2-3 % (Li et al., 2005). From all these separations, CH_4-CO_2 is the most expensive one since normally CO_2 content is higher than 25 %. The biogas composition of LFG depends on the waste composition and aging of the landfill (Shin et al., 2002). The composition of biogas generated in anaerobic digestion units of WWTPs depends on the sludge and the operation conditions of digestion process. Humidity, pH, temperature, and composition, particle size and age of the waste are factors that affect the biogas generation.

After the removal of minor contaminants, carbon dioxide and methane can be separated by physical or chemical scrubbing (Jacobson, 2009; Wellinger, 2009), membrane-based processes (Air Liquide), pressure swing adsorption (PSA) and temperature swing adsorption (TSA) (CarboTech; Grande and Rodrigues, 2007a, b; Knaebel and Reynhold, 2002; Xebec).

2.2. Pressure Swing Adsorption (PSA)

PSA is a well known separation technique (Ruthven et al., 1994; Sircar, 2002; Voss, 2005), in practice for at least 60 years (Skarstrom, 1960). A PSA process is cyclic in nature: after the adsorbent is saturated with the most adsorbed specie, a suitable protocol for regeneration should

be designed. In this gas separation process, one or more components of a gas mixture are preferentially adsorbed in a solid surface while the other(s) are not preferentially adsorbed. In a multicolumn process, the gas mixture is fed into the first adsorption column where it is purified and during this time the remaining columns were undergo regeneration. For that reason, there is always an adsorber column actively cleaning gas and therefore, the process is continuous. Generally, the regeneration is achieved by reducing the total pressure of system and introducing a gas at same pressure (PSA) or by increasing the temperature (TSA). In this separation process, the adsorbent can be used for a long period before the regeneration and as it operates at normal temperature and relatively low pressure, the energy consumption is low.

PSA technology can operate in two distinct modes, depending on the adsorbent employed (Grande and Rodrigues, 2007a; Ruthven et al., 1994; Yang, 1987). Some materials present stronger surface interactions with CO_2 adsorbing larger loadings of this gas when compared to methane. These materials are termed as equilibrium-based adsorbents and some examples are: activated carbon (Davis, et al., 1992; Sircar and Koch, 1986, 1988a), zeolite 13X (Sircar, et al., 1988b), silica gel (Dolan and Mitariten, 2003a) and metal-organic frameworks (Cavenati et al., 2008; Müller et al., 2005; Wang et al., 2002). Other materials have similar adsorption loadings of CO_2 and CH_4, but their diffusion rates can be controlled by tightening the size of the micropores. In materials like carbon molecular sieves (Masahiro and Kazuo, 1995), clinoptilolites (Jayaraman et al., 2004; Jayaraman et al., 2005; Seery, 1998), titanosilicates (Anson et al., 2009; Dolan and Mitariten, 2003b), DDR zeolites (Fujita et al., 2006) and SAPO-34 (Li et al., 2006) where kinetic separation takes place since much more CO_2 is adsorbed than CH_4 per unit time. The cycle configuration of a PSA process depends on the specific application. Different steps should be employed if the process intends to purify the less adsorbed compounds or if the target is to concentrate the most adsorbed one. The design of PSA depends strongly on the properties of the adsorbent: adsorption loading and diffusion, thermal effects, etc. When the kinetic diameter of the gas molecules is very close it is possible to select materials such that one molecule is larger than the pore diameter and is thus not adsorbed. This size-exclusion or molecular-gate concept is already applied for different separations: oxygen-nitrogen, carbon dioxide-methane, methane-nitrogen, etc (Cavenati et al., 2009; Farooq et al., 2002; Kuznicki et al., 1999, 2000; Mitariten, 2001, 2004).

3. Fundamental Concepts of Adsorption

Adsorption is the phenomenon that occurs when a molecule of a fluid (gas or liquid) is in contact with the surface of a solid; the fluid is called adsorbate and the surface is the adsorbent. The adsorbate molecules will form bonds with the adsorbent surface and become attached. So, the adsorption results of the unsaturated forces that act in the discontinuities existing in the adsorbent structure. This phenomenon, illustrated in Figure 3.1, is spontaneous, for this reason, we have always heat release. Its amount depends on the specific adsorbate-adsorbent system and on operating conditions.

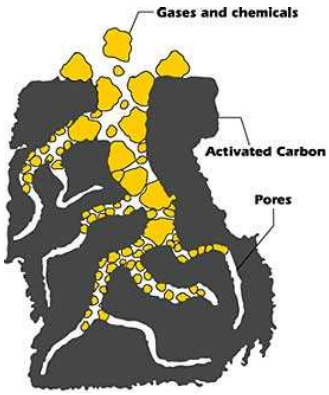

Figure 3.1. Activated Carbon adsorbs gases and chemicals. (Online Chemistry Portal, 2011)

The adsorption may be classified according to the adsorbate–adsorbent interactions, the chemical adsorption (chemisorption) and the physical adsorption (physisorption). The different kinds of adsorption bonds have different energy.

3.1. The Adsorbent

A good adsorbent is a solid that have good adsorptive capacity and good adsorption kinetics so, the solid must have a higher surface area or a micropore volume and must have a large pore network, that is, a high porosity (Do, 1998).

The range of pore size according to the classification recommended by IUPAC is: micropores ($d < 2$ nm), mesopores ($2 < d < 50$ nm) and macropores ($d > 50$ nm).

Alumina, silica gel, activated carbon and zeolite are the most common adsorbents; they are used in diverse processes. The most important characteristic of an adsorbent is its high porosity (Yang, 1987). So, physical characterization is generally more important than chemical characterization.

There are standard techniques to characterize porous material, for example, mercury porosimetry, liquid nitrogen adsorption, x-ray diffraction. If we have some of the mentioned

techniques we can measure the surface area, the total pore volume, the pore size distribution and crystal structure, for example. The surface area of an adsorbent can be determined using the adsorption data for nitrogen at liquid temperature, 77 K. The Brunaur-Emmet-Teller equation is used to calculate the amount of N_2 for monolayer coverage. The total pore volume is usually determined by helium and mercury densities while the pore size distribution is measured by mercury porosimetry for pores larger than 60 Å and by N_2 desorption (or adsorption) for pores in the range larger than 5 Å. The crystal structure is determined by x-ray diffraction.

3.1.1. Zeolites

Zeolites are crystalline materials that belong to the class of aluminosilicates, which may be constituted by alkali or alkali earth elements, such as sodium, potassium and calcium. The stoichiometric formula is represented by: $M_{x/n}[(AlO_2)_x(SiO_2)_y]zH_2O$ where x and y are integers, n is the valence of cation M and z is the number of water molecules in each unit cells. The tetrahedra of silicon and aluminium, SiO_4 and AlO_4, are the primary structural units. These atoms are connected through shared oxygen atoms raising an open crystal lattice. This crystalline framework contains cavities and channels into which the molecules can penetrate. About 150 types of zeolites have been synthesized, they are designated by letters. The main characteristic of these synthetic zeolite adsorbents are described in Table 3.1.

Table 3.1. Characteristic of major synthetic zeolite adsorbents. (Yang, 1987).

Zeolite Type	Major Cation	Nominal Aperture Size, Å	Bulk Density, $kg \cdot m^{-3}$	Water Capacity, %
3A (Linde)	K	3	600	20.0
3A (Davidson)	K	3	690	21.0
4A (Linde)	Na	4	615	22.0
4A (Davidson)	Na	4	660	23.0
5A (Linde)	Ca	5	675	21.5
5A (Davidson)	Ca	5	660	21.7
10X (Linde)	Ca	8	660	31.6
13X (Linde)	Na	10	570	28.5
13X (Davidson)	Na	10	645	29.5

The zeolite structure may be a set of cubes, hexagonal prisms, octahedra and truncated octahedra. The truncated octahedron is the structure unit of zeolites A and X and the zeolite type X has a larger pore than type A.

In this adsorbent the gas separation is based on the different adsorption equilibrium of the gases.

3.1.2. Carbon Molecular Sieves (CMS)

Carbon molecular sieves are a modified type of carbon activated with a more uniform pore size distribution and a pore size of several angstroms (Jüntgen, et al., 1981), the effective micropore diameters of CMS may range from 4 to 9 angstroms (Ruthven, 1984). These materials have a high internal surface area/equilibrium capacity and a partial/total molecular sieving capability (Srinivasan et al., 1995). The synthesis of these carbons has as a final objective to obtain a material with a homogeneous pore size distribution. The carbonization of the coal and the coating of coke on the coal char are the basics procedures in their synthesis, the pyrolysis and activation steps are determinant in the micropore size (Jüntgen et al., 1981). The carbon molecular sieves are bidisperse adsorbents featuring micropores smaller than 10 Å and macropores between 0.1-1 µm (Schröter, 1993; Grande et al., 2003) however, the controlling resistance is almost located in the micropores (Qinglin et al., 2003).The gas separation in this type of adsorbent is based on the different adsorption kinetics of the gases although have similar adsorption loadings.

3.2. Models for the Description of the Gas Adsorption Equilibrium

The contact between an adsorbent and an adsorbate, at a given temperature and pressure, leads to an equilibrium relation between the adsorbed amount and the adsorbate concentration in the fluid phase. The representation of these data is termed adsorption isotherms.

3.2.1. The Langmuir Model

This model is based on a kinetic point of view, that equals the rate of adsorption to the rate of desorption from the surface at equilibrium (Do, 1998). This model assumes that:

- the surface is homogeneous, that is, the adsorption energy is constant in all sites;
- the adsorption in surface is localized, that is, adsorbed atoms or molecules are adsorbed;
- each site can accommodate only one molecule or atom;

- there is no lateral interaction between adsorbed molecules.

The Langmuir isotherm is expressed by the equation 3.1.

$$q_i^* = q_{i,max} \frac{K_i P}{1 + K_i P} \tag{3.1}$$

where, q_i^* is the amount of the adsorbed phase of component *i*, $q_{i,max}$ is the maximum adsorbed amount of component *i*, corresponding to a complete monolayer coverage, K_i is the affinity constant or Langmuir constant and P is the gas pressure.

The Langmuir model can take the following two forms if:

- the pressure is very low → $1 >> K_i P$ → the isotherm reduces to the Henry Law:

$\frac{q_i^*}{q_{i,max}} = K_i P$, that is, the amount adsorbed increases linearly with the pressure.

- the pressure is relatively high → $K_i P >> 1$ → the amount adsorbed reaches the saturation capacity, all sites are occupied (is called monolayer coverage, $\frac{q_i^*}{q_{i,max}} = 1$).

3.2.2. The Freundlich Model

This model considers the adsorption on nonuniforms surfaces, the adsorbate can occupies *n* sites. The resulting isotherm is expressed by:

$$q_i^* = q_{i,max} \frac{(K_i P)^{1/n_i}}{1 + (K_i P)^{1/n_i}} \tag{3.2}$$

where q_i^* is the amount of the adsorbed phase of component *i*, $q_{i,max}$ is the maximum adsorbed amount of component *i* and n_i represents the adsorbent heterogeneity.

The Freundlich equation does not have a proper Henry law behaviour at low pressure and when this is sufficiently high, it does not have a finite limit (Do, 1998). According to this isotherm, the amount adsorbed will increase indefinitely with the pressure.

3.2.3. The Toth Model

The Toth equation (Toth, 1971) is an empirical isotherm equation but does not have the same limitations like the others empirical equations as Freundlich and Sips equations. The Sips isotherm has the same problem at low pressure and does not have a proper Henry law behavior. This equation describes many systems with sub-monolayer coverage:

$$q_i^* = q_{i,max} \frac{K_i P}{\left[1 + (K_i P)^{n_i}\right]^{1/n_i}} \tag{3.3}$$

where q_i^* and $q_{i,max}$ are the absolute amount adsorbed and the maximum amount adsorbed of component *i*, *P* is the gas pressure and n_i is the heterogeneity parameter.

The adsorption constant (K_i) is assumed to have an exponential dependence of temperature according to:

$$K_i = K_i^0 \exp\left(-\frac{\Delta H_i}{R_g T}\right) \tag{3.4}$$

$$n_i = A_i + B_i T \tag{3.5}$$

where K_i^0 is the infinite adsorption constant, ΔH_i is the isosteric heat of adsorption at zero loading, *T* is the temperature, R_g is the universal gas constant and A_i and B_i are the parameters relating the thermal variation of the heterogeneity coefficient. The parameters K_i and n_i are specific for adsorbate–adsorbent pairs and the last is less than the unity. This parameter is used to characterize the adsorbent and when it decreases means that the material is more heterogeneous.

3.2.4. The Multi-Site Langmuir or Nitta Model

The multisite Langmuir model represented in Equation (3.6) assumes that a molecule can occupy more than one adsorption site of a homogenous surface.

$$\left(\frac{q_i^*}{q_{i,\max}}\right) = K_i P y_i \left[1 - \frac{q_i^*}{q_{i,\max}}\right]^{a_i} \tag{3.6}$$

where q_i^* and $q_{i,max}$ are the current and the maximum amount adsorbed of component i for a given pressure *P* and a constant solid temperature T_s. The exponent a_i corresponds to the number of neighbouring sites that a molecule can occupy. The adsorption constant (K_i) is determined by the equation 3.4. If we neglect adsorbate-adsorbate interactions, the multicomponent extension of this model can be expressed as:

$$\left(\frac{q_i^*}{q_{i,\max}}\right) = K_i P y_i \left[1 - \sum_i \left(\frac{q_i^*}{q_{i,\max}}\right)\right]^{a_i} \tag{3.7}$$

The saturation capacity of each component is imposed by the thermodynamic constraint, $a_i q_{i,max} = constant$ to satisfy a material balance of sites in the adsorbent (Sircar, 1995).

3.3. Adsorption kinetics. Diffusion in Porous Media

The rates of adsorption and desorption in porous adsorbents are generally controlled by transport within the pore network and not by the intrinsic kinetics of sorption at the surface (Ruthven, 1984). Like the bulk gas phase through the pores is generally little, it is possible to consider intraparticle transport as a diffusive process, that is, it is assumed that when a molecule enters into an adsorbent ('in micropores'), it will only collide with the solid and will not be part of a gas phase; so, it is possible to correlate the kinetic data in terms of diffusivity defined in accordance with Fick's first equation:

$$J = -D(c)\frac{\partial c}{\partial x} \tag{3.8}$$

where c is the concentration in $mol \cdot m^{-3}$, D is the diffusion coefficient or diffusivity in $m^2 \cdot s^{-1}$, J is the diffusion flux in $mol \cdot m^{-1} \cdot s^{-1}$ and x is the position in m.

This law relates that the flux goes from regions of high concentration to regions of low concentration. The pore diffusion may occur by several different mechanisms depending on the pore size, the sorbate concentration and other conditions (Ruthven, 1984). In fine micropores, like the intracrystalline pores of zeolites, the diffusing molecule never escapes from the force field of the adsorbent surface therefore; this process is often called surface diffusion. Normally, the terms micropore or intracrystalline diffusion are used to describe the transport in micropores, when the diffusing molecule escapes from the surface field (in large pores), the diffusion is called macropore diffusion.

In macropore mass transfer may occur three distinct mechanisms of transport (Ruthven, 1984): molecular diffusion, Knudsen diffusion and Poiseuille flow, which are represented in Figure 3.2.

3.3.1. Molecular Diffusion

It occurs when the resistance to mass transfer is a result of collision between diffusing molecules. The molecular diffusion will be the dominant transport mechanism when the average distance travelled between molecular collisions is small relative to the pore diameter, which can be seen in Figure 3.2a).

If the transport within the macropores occurs only by molecular diffusion, the pore diffusivity ($D_{p,i}$) is given by:

$$D_{p,i} = \frac{D_{m,i}}{\tau_p} \tag{3.9}$$

where $D_{m,i}$ is the molecular diffusivity and can be estimated from the Chapman-Enskog equation and τ_p is the tortuosity factor.

For a binary gas mixture the Chapman-Enskog equation is used to determine the molecular diffusivity ($D_{m,i}$) expressed in $cm^2 \cdot s^{-1}$:

$$D_{m,i} = \frac{0.0018583 T^{3/2} \left(\frac{1}{M_1} + \frac{1}{M_2} \right)^{1/2}}{P \sigma_{12}^2 \Omega_{12}} \tag{3.10}$$

where M_1 and M_2 are the molecular weights, P is the total pressure in atmospheres and Ω is the collision integral and function of ε / kT , where k is the Boltzmann constant.

The Lennard-Jones force constant, ε is given by:

$$\varepsilon = \sqrt{\varepsilon_1 \varepsilon_2} \tag{3.11}$$

The collision diameter from the Lennard-Jones potential, σ_{12}, expressed in Angstroms is calculated by:

$$\sigma_{12} = \frac{1}{2}(\sigma_1 + \sigma_2) \tag{3.12}$$

3.3.2. Knudsen Diffusion

This transport mechanism occurs when mean free path is greater than the pore diameter consequently, the collisions between molecule and pore wall is the main diffusional resistance, and this mechanism is represented in Figure 3.2b).

The Knudsen diffusivity ($D_{k,i}$), expressed in $cm^2 \cdot s^{-1}$, can be estimated from the equation:

$$D_{K,i} = 9700 r_p \left(\frac{T}{M_w} \right)^{1/2} \tag{3.13}$$

where M_w is the molecular weight, r_p is the mean pore radius in cm and T is the temperature in Kelvin.

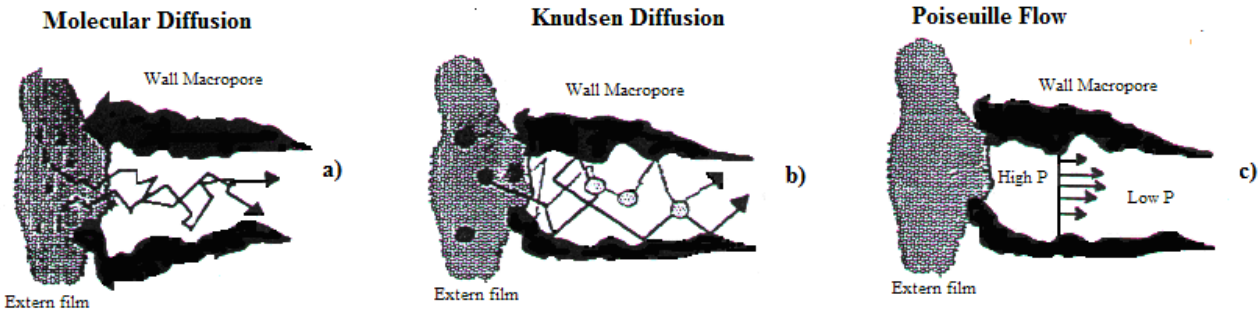

Figure 3.2. Mechanisms of diffusion on macropore: a) Molecular Diffusion; b) Knudsen Diffusion; c) Poiseuille Diffusion. (Ruthven, 1996)

3.3.3. Poiseuille Flow

This mechanism is present when there is a difference in total pressure across a particle, and consequently there will be a direct contribution to the adsorption flux from forced laminar flow through the macropores, as can be seen in Figure 3.2c).

From Poiseuille's equation it may be shown that the equivalent diffusivity, expressed in $cm^2 \cdot s^{-1}$, is given by:

$$D = \frac{P r_p^2}{8\mu} \tag{3.14}$$

where P is the total pressure in $dynes \cdot cm^{-2}$, r_p is the mean pore radius in cm and μ is the viscosity in poise.

3.3.4. Micropore diffusion and Pore-mouth resistance in micropores

The diffusion of gases into the adsorbent particles until its adsorption in the surface involves different transfer mechanisms: the gas has to diffuse through distribution channels (macropores) and then diffuse inside the micropores before they reach their adsorption location.

Normally, the diffusion within zeolites crystals can be simplified to a Linear Driving Force (LDF) model. For the case of crystal diffusion, the micropore LDF constant ($k_{\mu,i}$) assumes the same exponential dependence of temperature (Ruthven, 1984) as micropore diffusion:

$$K_{u,i} = K_{u,i}^0 \exp\left(-\frac{Ea_i}{R_g T}\right) \tag{3.15}$$

where $K_{u,i}^0$ is the LDF constant for infinite temperature and Ea_i is the energy of activation.

For the case of carbon molecular sieves, also bidisperse adsorbents, the micropores and macropores resistances are distinct. However, in the mostly gas separations the controlling resistance is located in the micropores (Farooq et al., 2002). Three types of diffusion mechanism in micropores may be encountered: distributed pore diffusional resistance (Chagger et al., 1995; Chen et al., 1994; Liu and Ruthven, 1996; Rutherford and Do, 2000; Ruthven, 1992; Ruthven et al., 1986; Van Den Broeke and Krishna, 1995), barrier resistance confined at the pore mouth (Dominguez et al., 1988; Fitch et al., 1994; LaCava et al., 1989; Liu and Ruthven, 1996; Reid and Thomas, 1999, 2001; Rynders et al., 1997; Srinivasan et al., 1995), or a dual resistance model (Liu and Ruthven, 1996; Loughlin et al., 1993; Reid and Thomas, 1999, 2001) which is a combination of micropore resistance and surface barrier at the mouth of the micropores. The micropore LDF constant is composed by the micropore diffusion resistance and the surface barrier at the mouth of the micropores and can be described by (Cavenati et al., 2005) the equation 3.16:

$$K_{u,i} = \frac{1}{\frac{1}{K_{b,i}} + \frac{r_c^2}{15 D_{u,i}^{\infty}}} \tag{3.16}$$

The temperature dependence of micropore diffusion and surface barrier at the mouth of the micropores can be described by the following equations:

$$D_{u,i}^{\infty} = D_{u,i}^{0} \exp\left(-\frac{Ea_i}{R_g T}\right) \tag{3.17}$$

$$K_{b,i} = K_{b,i}^{0} \exp\left(-\frac{Eb_i}{R_g T}\right) \tag{3.18}$$

where $K_{u,i}^{0}$ is the LDF constant for infinite temperature, $D_{u,i}^{\infty}$ is the micropore diffusivity of component *i* at infinite dilution, $D_{u,i}^{0}$ diffusivity of component *i* at infinite temperature, Ea_i is the energy of activation of component *i*, Eb_i is the activation energy for micropore barrier resistance of component *i*, $K_{b,i}$ is the barrier mass transfer coefficient of component *i* and $K_{b,i}^{0}$ is the micropore barrier resistance at infinite temperature of component *i*.

4. Modelling of Pressure Swing Adsorption

A classical Pressure Swing Adsorption (PSA) unit is composed by several columns operating in parallel filled with one selective adsorbent. However, the configuration of PSA units is so flexible that we can find units with only one column (Siettos et al., 2003) or with multiple adsorbents per column (Cavenati et al., 2006a; Grande and Rodrigues, 2007b; Lü et al. 2003, 2004; Ribeiro et al., 2008).

When a PSA is designed for an application, the first difficulty to overcome is the selection of the adsorbent. As mentioned before, kinetic adsorbents are normally selected for bulk separation of CO_2. Nonetheless, it was mentioned by several researchers that zeolites adsorbents can also provide an alternative. In Chapter 5, zeolite 13X was selected since under certain operating conditions, faster regeneration can be carried out. In Chapter 6 and taking into account the main chapter objective, to find a new cycle to enhance the kinetic adsorbents performance, the carbon molecular sieve 3K was the adsorbent chosen.

4.1. Adsorption equilibrium and kinetics

The basic information to simulate and design a PSA process is the pure gas adsorption equilibrium and diffusion kinetics in the adsorbent. While the adsorption equilibrium of CO_2 and CH_4 on zeolite 13X (CECA, France) was determined in a magnetic suspension balance (Rubotherm, Germany), the data of pure gases on CMS-3K (Takeda, Japan) was already available (Cavenati et al., 2005). The adsorption equilibrium of CO_2 and CH_4 on zeolite 13X is reported in Figure 4.1.

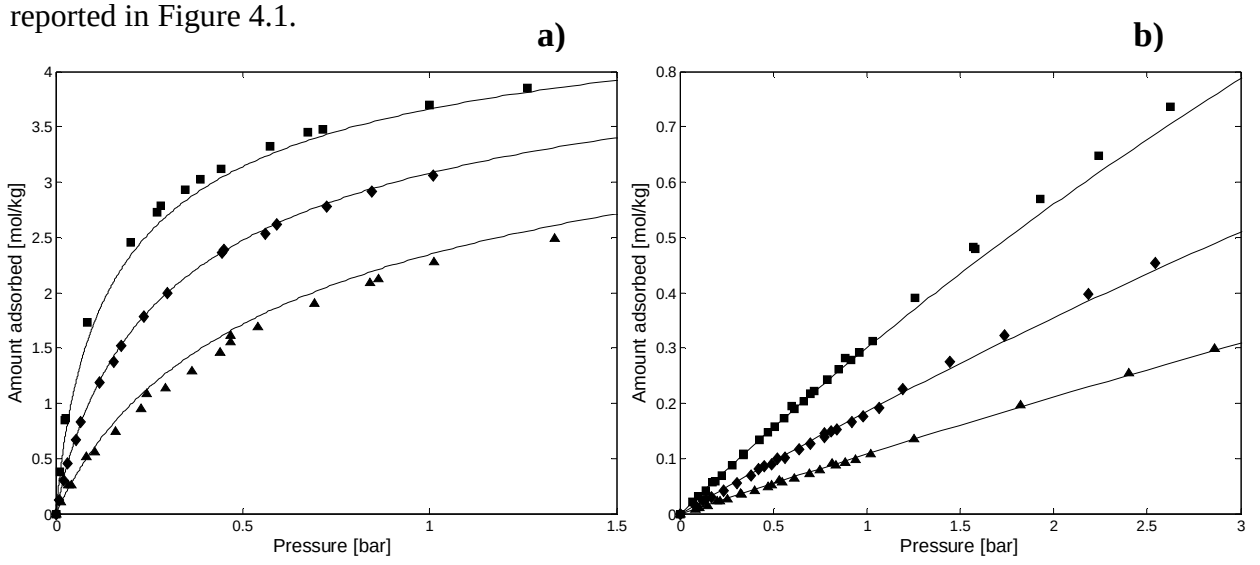

Figure 4.1. Adsorption equilibrium isotherms on zeolite 13X of (a) CO_2 and (b) CH_4. ■, T=303; ♦, T=323 and ▲, T=348 K.

Solid lines in Figure 4.1 correspond to the fitting of the multisite Langmuir model (Nitta et al., 1984), which is described in chapter 3.2.4.

The parameters obtained from fitting of pure adsorption equilibrium are shown in Table 4.1, as well as the adsorption equilibrium of CO_2 and CH_4 on CMS-3K. The kinetic parameters of pure gases on zeolite 13X and CMS-3K are also presented in this table.

Table 4.1. Adsorption equilibrium and kinetic parameters of CH_4 and CO_2 adsorption on zeolite 13X (Santos et al, 2011) and CMS-3K. (Cavenati et al, 2005)

Gas	$q_{i,max}$ (mol·kg^{-1})	K_i^0 (Pa^{-1})	$-\Delta H$ (J·mol^{-1})	a_i (-)	Ea_i (J·mol^{-1})	$K_{u,i}^0$ (m^2·s^{-1})	Eb_i (J·mol^{-1})	$K_{u,i}^0$ (s^{-1})	$D_{u,i}^0 / r_c^2$ (s^{-1})
Zeolite 13X									
CO_2	5.305	2.93×10^{-10}	31,164	1.962	21,008	$1.74\text{x}10^{-11}$			
CH_4	6.411	1.29×10^{-10}	20,856	1.624	6,621	$2.52\text{x}10^{-12}$			
CMS-3K									
CO_2	8.974	1.73×10^{-11}	38,947	8.287	25,551				22.12
CH_4	11.797	2.48×10^{-13}	33,674	6.303	35,271		41,212	268.7	2.77

4.2. Mathematical modelling of fixed-bed column

The mathematical model of a column filled with adsorbent is described by a set of partial differential equations including mass, energy and momentum balances. For some specific cases, these equations can be simplified (constant velocity or isothermal behaviour), however for bulk gas-phase separations, all these equations are normally required (Ruthven, 1994; Yang, 1987).

In this work, the mathematical model used to describe the fixed-bed adsorption column is based on the following assumptions (Da Silva et al., 1999; Da Silva and Rodrigues, 2001):

- The gas phase behaves as an ideal gas;
- Mass, heat and momentum variations in the radial direction are negligible;
- The mass transfer rate is represented by a bi-linear driving force (bi-LDF) model;
- A film mass transfer in the layer surrounding the extrudates is considered;

- The pressure drop in the column is described by Ergun Equation;
- The bed porosity is considered constant along the bed;
- The process runs under adiabatic operation;
- Heat conduction through the column wall can be neglected.

The assumption of negligible influence of the heat conduction through the column wall is based in the slow dynamics of the heat conduction through the column wall when compared to the dynamics of the mass balance in the column.

The mathematical model proposed (Da Silva et al., 1999; Da Silva and Rodrigues, 2001) was validated against experimental data of breakthrough curves and single-column PSA separation of CH_4-CO_2 using zeolite 13X (Cavenati et al., 2005).

The component mass balance for the gas phase in the adsorption column is given by:

$$\frac{\partial}{\partial z}(\varepsilon_c D_{ax} C_T \frac{\partial y_i}{\partial z}) - \frac{\partial}{\partial z}(u_0 C_i) = \varepsilon_c \frac{\partial C_i}{\partial t} + \frac{(1-\varepsilon_c) a_p k_{f,i}}{(1+Bi_i/5)}(C_i - \langle C_{p,i} \rangle) \tag{4.1}$$

where C_T is the total gas-phase concentration, C_i is the gas-phase concentration of component i, D_{ax}, is the axial dispersion coefficient, u_0 is the superficial velocity, ε_c is the column porosity, $k_{f,i}$ is the film mass-transfer resistance for component i, $\langle C_{p,i} \rangle$ is the averaged concentration of component i in the macropores of the adsorbent and a_p is the extrudate specific area.

In this equation the Biot Number of component i is defined as:

$$Bi_i = \frac{k_{f,i} R_p^2}{\varepsilon_p D_{p,i}} \tag{4.2}$$

where R_p is the extrudate radius, $D_{p,i}$ is the pore diffusivity of component i and ε_p is the pellet porosity.

When the LDF approximation is used to describe mass transfer rate within the large pores of the matrix, the mass balance for extrudate is given by:

$$\frac{\partial \langle C_{p,i} \rangle}{\partial t} = \frac{15 D_{p,i}}{R_p^2} \frac{1}{(1+5/Bi_i)}(C_i - \langle C_{p,i} \rangle) - \frac{\partial \langle \overline{q}_i \rangle}{\partial t} \frac{\rho_p}{\varepsilon_p} \tag{4.3}$$

where ρ_p is the particle density, and $\langle \overline{q}_i \rangle$ is the extrudate-averaged adsorbed-phase concentration of component i. The pore diffusion coefficient, $D_{p,i}$ was estimated assuming contribution of molecular and Knudsen diffusion with a tortuosity factor of 2.0 (Da Silva et al., 1999; Da Silva and Rodrigues, 2001).

The mass transfer rate in micropores is also described by a LDF approximation given by:

$$\frac{\partial\langle\bar{q}_i\rangle}{\partial t}=\frac{15D_{c,i}}{r_c^2}(q_i^*-\langle\bar{q}_i\rangle)=K_{u,i}(q_i^*-\langle\bar{q}_i\rangle) \tag{4.4}$$

where $D_{c,i}$ is the crystal diffusivity of component *i*, r_c is the crystal radius, and q_i^* is the gas-phase concentration of component *i* in equilibrium with the gas concentration within the micropores, $\langle C_{p,i}\rangle$.

The superficial velocity is related to the total pressure gradient by Ergun Equation:

$$-\frac{\partial P}{\partial z}=\frac{150\mu(1-\varepsilon_c)^2}{d_p^2\varepsilon_c^3}u_0+\frac{1.75(1-\varepsilon_c)\rho_g}{d_p\varepsilon_c^3}|u_0|u_0 \tag{4.5}$$

where P is the total pressure, μ is the gas viscosity, d_p is the particle diameter, and ρ_g is the gas density.

To take into account the energy transfer, three different balances were employed: gas, solid and column wall. The energy balance for the gas phase is expressed by:

$$\varepsilon_c C_T\tilde{C}v\frac{\partial T_g}{\partial t}=\frac{\partial}{\partial z}\left(\lambda\frac{\partial T_g}{\partial z}\right)-u_0C_T\tilde{C}_p\frac{\partial T_g}{\partial z}+\varepsilon_cR_gT_g\frac{\partial C_T}{\partial t}-(1-\varepsilon_c)h_fa_p(T_g-T_s)-\frac{2h_w}{R_w}(T_g-T_w) \tag{4.6}$$

where $\tilde{C}v$ is the molar constant volumetric specific heat of the gas mixture, T_g is the temperature of the gas phase, T_s is the solid (extrudate) temperature, T_w is the wall temperature, λ is the axial heat dispersion, $\tilde{C}_p$ is the molar constant pressure specific heat of the gas mixture, h_f is the film heat-transfer coefficient between the gas and solid phases, h_w is the film heat-transfer coefficient between the gas phase and the column wall, R_w is the column radius.

The energy balance in the solid phase is given by:

$$\begin{aligned}&(1-\varepsilon_c)\left[\varepsilon_p\sum_{i=1}^{n}\langle C_{p,i}\rangle\tilde{C}_{vi}+\rho_p\sum_{i=1}^{n}\langle\bar{q}_i\rangle\tilde{C}_{v,ads,i}+\rho_p\tilde{C}_{p_s}\right]\frac{\partial T_s}{\partial t}=\\&(1-\varepsilon_c)\varepsilon_pR_gT_s\frac{\partial\langle C_{p,i}\rangle}{\partial t}+\rho_b\sum_{i=1}^{n}(-\Delta H_{ads,i})\frac{\partial\langle\bar{q}_i\rangle}{\partial t}+(1-\varepsilon_c)h_fa_p(T_g-T_s)\end{aligned} \tag{4.7}$$

where $\tilde{C}_{p_s}$ is the constant volumetric specific heat of component i, $\tilde{C}_{vi}$ is the molar constant volumetric specific heat of component i, $\tilde{C}_{v,ads,i}$ is the molar constant volumetric specific heat of component i adsorbed, ρ_b is the bulk density and $(-\Delta H_i)$ is the isosteric heat of adsorption.

For the column wall, the energy balance is described by:

$$\rho_w \tilde{C}_{pw} \frac{\partial T_w}{\partial t} = \alpha_w h_w (T_g - T_w) - \alpha_{wl} U (T_w - T_\infty) \tag{4.8}$$

where $\tilde{C}_{pw}$ is the specific heat of the column wall, U is the global external heat-transfer coefficient, and T_∞ is the environment temperature. In this equation, α_w is the ratio of the internal surface area to the volume of the column wall, α_{wl} is the ratio of the logarithmic mean surface area of the column shell to the volume of the column wall, that are defined by:

$$\alpha_w = \frac{d_{wi}}{e(d_{wi} + e)} \tag{4.9}$$

$$\alpha_{wl} = \frac{1}{(d_{wi} + e)\ln(\frac{d_{wi} + e}{d_{wi}})} \tag{4.10}$$

The mass and heat parameters employed in this model were estimated using correlations existing in literature (Bird et al., 2002; Ruthven, 1984; Wakao and Funazkri, 1978; Wasch and Froment, 1972).These correlations are summarized in Appendix A, Table A.1.

4.3. Modified Skarstrom cycle and performance variables

The operation of a PSA unit is not steady but cyclic: prior to massive breakthrough of the most adsorbed compound (CO_2), the adsorbent should be regenerated. To handle this requirement in continuous feed processing, several columns are employed: when one column is in feed mode, the other(s) are in regeneration. The regeneration procedure is also performed in different steps, intending to speed-up the removal of the adsorbed components.

In this work, the PSA cycle employed was a modified Skarstrom cycle (Kim et al., 2006) including pressure equalization. The steps are:

1. Co-current pressurization with feed to condition the pressure to start a new cycle;
2. Co-current feed, where selective removal of CO_2 takes place;
3. Co-current pressure equalization depressurization. In this step, the column is partially depressurized and the exiting gas is recycled to other column to save energy;
4. Counter-current blowdown where the pressure is reduced to the lower pressure of the cycle. Removal of CO_2 starts in this step;
5. Counter-current purge with product to displace CO_2 from the product-end of the column;
6. Counter-current pressure equalization recycling the gas exiting step 3 from other column to partially increases the pressure of the column.

A schematic representation of this cycle for a single column as well as the pressure history over one cycle is shown in Figure 4.2.

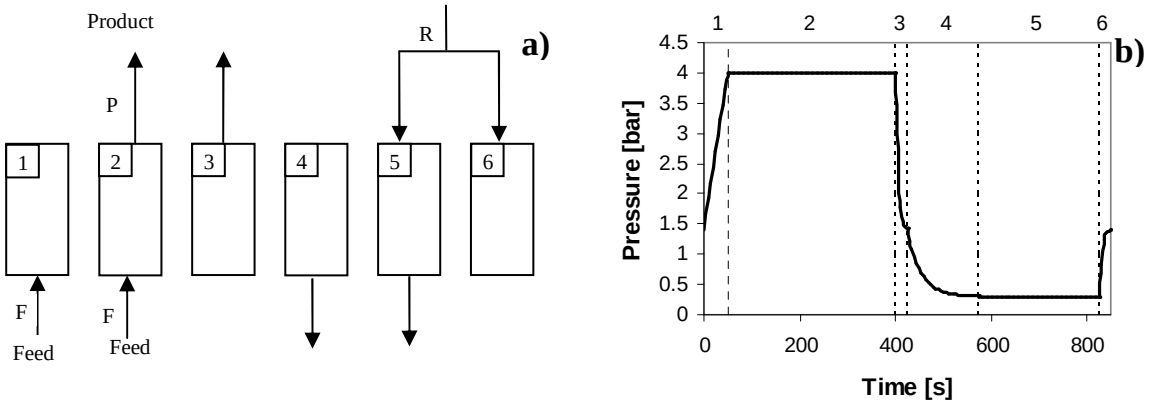

Figure 4.2. PSA cycle scheme (a) and pressure history of one CSS cycle (b) for a six steps 1-column PSA simulation. Steps are: 1) co-current feed pressurization, 2) adsorption, 3) co-current pressure equalization depressurization, 4) counter-current blowdown, 5) counter-current purge and 6) counter-current pressure equalization pressurization.

Simplified simulations of PSA cycles are carried out using this 1-column scheme: the inlet streams of steps 5 and 6 (purge and pressure equalization) are not recycled from the feed stream avoiding links between different columns and also saving variables making simulations faster. In 1-column process, the streams used in the purge and pressure equalization steps (5 and 6, respectively) were pure methane. A more realistic description of the system involves the simulation of all the columns comprised in the PSA unit. Note that in the 1-column simulations, the gas exiting step 3 is not considered as product and is also not recycled into any column. The results obtained using this strategy do not have any gas recycled into the column and also let us evaluate the increase of product recovery by using one equalization step. For a two-column PSA unit, the schematic representation is given in Figure 4.3 together with a pressure history. Simulations of multiple columns were performed for H_2 production indicating some variations in the performance (Nikolic et al., 2008, 2009; Ribeiro et al., 2008).

In this particular case, the specification of 98 % purity for CH_4 indicate that the recycled feed stream may contain large amounts of CO_2 which may seriously deviate the behaviour of the one-column simulations from real performance.

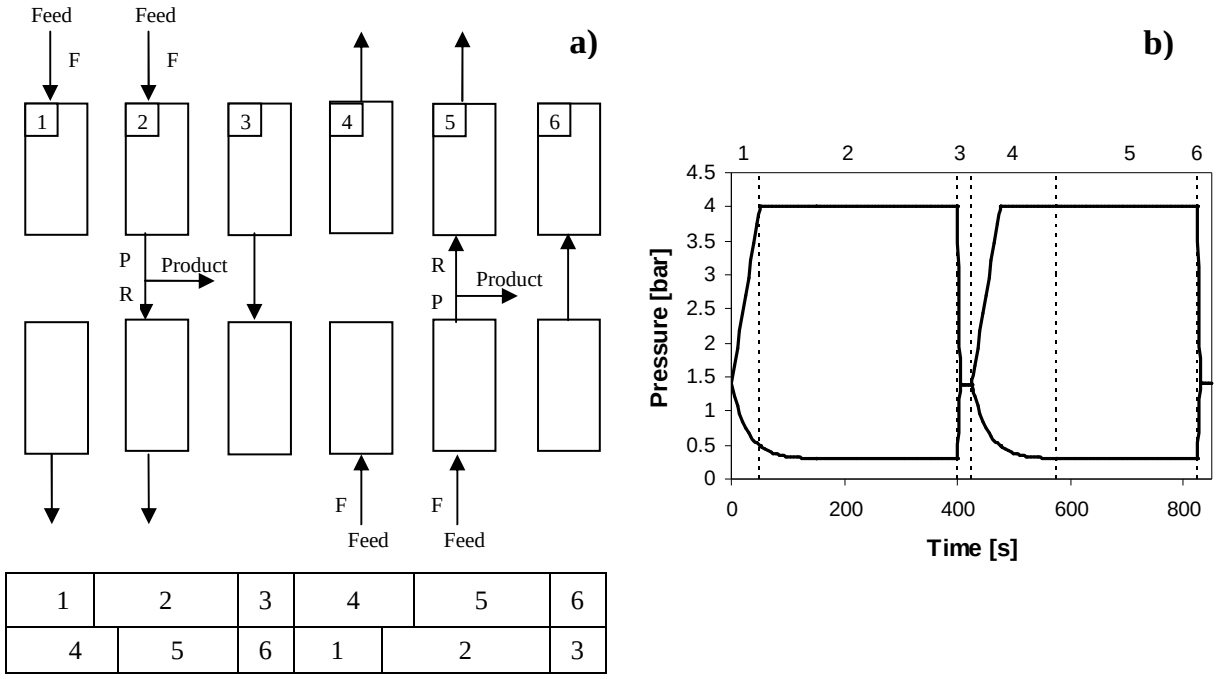

1	2	3	4	5	6
4	5	6	1	2	3

Figure 4.3. PSA cycle scheme (a) and pressure history of one CSS cycle (b) for a six steps 2-column PSA simulation. Steps are: 1) co-current feed pressurization, 2) adsorption, 3) co-current pressure equalization depressurization, 4) counter-current blowdown, 5) counter-current purge and 6) counter-current pressure equalization pressurization.

Four different parameters were used to evaluate the process performance, which depends to the cycle configuration used. These parameters are: product (CH_4) purity and recovery, unit productivity and power consumption. Product purity is defined for the stream exiting the feed step by:

$$Purity = \frac{N_{CH_4}}{N_{CH_4} + N_{CO_2}} \tag{4.11}$$

where N_{CH_4} is the number of moles of methane that exits the column in the feed step, the product, and N_{CO_2} is the amount of CO_2 impurities that exits the column in the feed step.

The CH_4 recovery is defined by the ratio between the number of moles of methane obtained as product divided by the number of moles of CH_4 introduced in feed (and pressurization steps).

$$\text{Recovery} = \frac{N_{CH_4} - R_{CH_4}}{F_{CH_4}} \tag{4.12}$$

where R_{CH_4} is the number of moles of methane that is recycled in the purge and pressure equalization steps and F_{CH_4} is the number of moles of methane fed to the column in the feed step.

The CH_4 productivity is calculated by:

$$Productivity = \frac{F_{CH_4} Recovery}{t_{total} w_{ads}} \tag{4.13}$$

where t_{total} is the total cycle time and w_{ads} the adsorbent mass.

The power consumption is defined as the required energy for compression of the different streams and the energy requirements of the PSA unit; it is calculated by adiabatic compression given by:

$$Power\ Consumption = \left(\frac{\gamma}{\gamma - 1}\right) R_g T_{feed} \left[\left(\frac{P_{high}}{P_{low}}\right)^{\left(\frac{\gamma-1}{\gamma}\right)} - 1\right] \times \frac{\dot{B}}{1000\eta} \tag{4.14}$$

where $\gamma = \tilde{C}_p / \tilde{C}_v$ (equal to 3/2 for ideal gases), R_g is the universal gas constant, P_{high} is the discharge pressure, P_{low} is the suction or blowdown pressure, $\dot{B}$ is the molar flowrate to be compressed, and η is the mechanical efficiency, which typically assumes a value of 0.8. For the compression of methane from 4 to 200 bar, γ =1.31 was employed. The power consumption was estimated assuming that the mixture CH_4/CO_2 was available at 1 bar and will be compressed to the feed pressure (4 bar), followed by further compression of the product (CH_4) to 200 bar. The specific use of energy in the PSA cycle is given by the blowdown and purge steps.

The existence of different cycle steps, imply that different boundary conditions exist to solve the mathematical model presented previously. The different boundary conditions for each of the steps employed in the PSA cycle as well as initial conditions are listed in Appendix B, Table B.1. In this study, it was assumed that the adsorption beds were at constant temperature (323 K) filled with an inert gas at a pressure of 1.2 bar.

The model described by the equations 4.1-4.10 was solved using gPROMS software (PSE Enterprise, UK). The centered finite difference method (CFDM) of second order over a uniform grid of 250 intervals was the numerical method used. The solvers employed in the simulations used a value of 1×10^{-5} for absolute tolerance.

5. Simulation of a PSA Process for Biogas Upgrading

The purpose of this chapter is to design a PSA unit for biogas upgrading and to evaluate the effect of recycling streams in purge and equalization steps with some content of contaminant (CO_2). The biogas stream has a total flowrate of 500 $Nm^3 \cdot day^{-1}$ (at 296.15 K and 1 atm) with a content of CO_2 of 33 % balanced by CH_4. The biogas is available at 323 K and at atmospheric pressure and should be compressed to the feed pressure (4 bar). For this purpose, one and two column PSA simulations were performed.

5.1. PSA sizing

The diameter of the PSA process was designed in order to have superficial velocity lower than 0.2 $m \cdot s^{-1}$ in the feed step in order to allow a reasonable gas solid contact time and reduce effects of axial dispersion. The length of the column was fixed to have a feed time shorter than 10 minutes. The physical properties of the adsorbent, zeolite 13X, are shown in Table 5.1 and all properties of the column as well as the operation conditions are described in Table 5.2. The simulations were also carried out assuming that the columns will operate under adiabatic behaviour (U=0). However, some heat is exchanged with the column wall (h_w=35 $W \cdot m^{-2} \cdot K$). Under this regime, temperature excursion within the column (due to adsorption / desorption) will be the highest attainable and thus will establish a lower limit of operation: if there is some energy exchange with the surroundings, the temperature excursion will be smaller and PSA performance will be better.

Table 5.1. Physical properties of zeolite 13X used in the breakthrough and PSA simulations.

Adsorbent property	Zeolite 13X
Pellet density ($kg \cdot m^{-3}$)	1,324
Pellet porosity	0.338
Pellet radius (m)	0.0006
Pellet tortuosity	2.0
Mean pore radius (A)	243[a]
Zeolite 13X specific heat ($J \cdot kg^{-1} \cdot K^{-1}$)	900

[a]This value was obtained by Mercury Intrusion Porosimetry.

Table 5.2. Column characteristics and operating conditions used in the breakthrough and PSA simulations.

Column length (m)	1.35
Column radius (m)	0.10
Column porosity	0.37
Column wall specific heat ($J \cdot kg^{-1} \cdot K^{-1}$)	500
Column density ($kg \cdot m^{-3}$)	834.12
Column wall density ($kg \cdot m^{-3}$)	8,238
Feed flowrate (SLPM)	347.2
Pressure feed (bar)	4.0
Temperature feed (K)	323.15

As example of the behaviour of the column, in Figure 5.1 the simulation of a breakthrough curve for CH_4/CO_2 stream is presented. During the bulk CO_2 adsorption within the column, the temperature increase is higher than 60 K. The adiabatic behavior also produces a second plateau in the molar flowrate profile of CO_2 (Basmadjian, 1997). The higher temperature within the bed resulted in a decreased overall capacity.

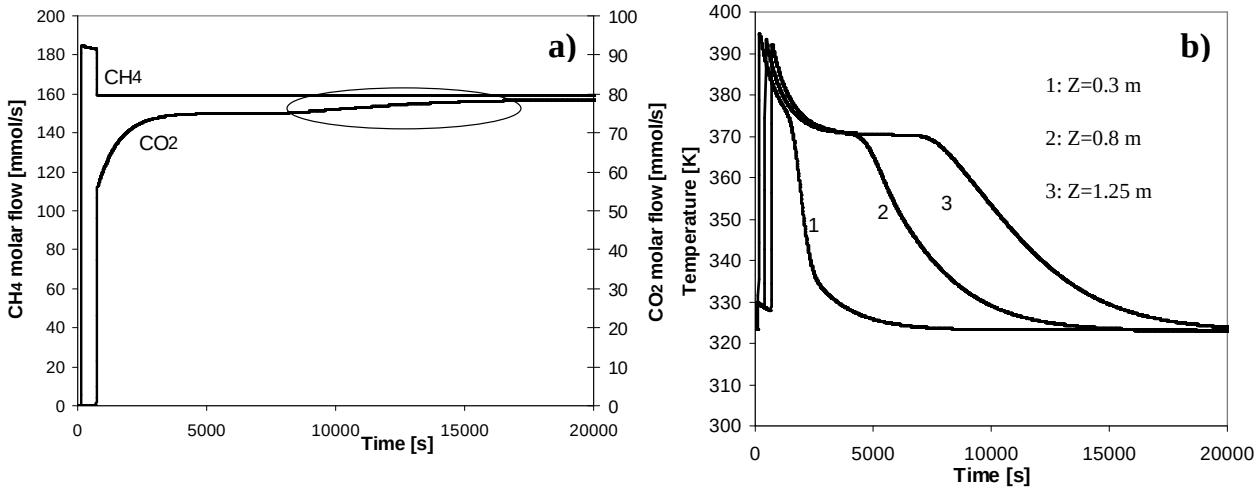

Figure 5.1(a) Molar flowrate of CH_4 and CO_2 and (b) temperature profiles at 0.3, 0.8 and 1.25 m from feed inlet for a simulated binary curve (67 % of CH_4 balanced by CO_2) at 323 K, 4 bar with a total feed flowrate of 347.2 SLPM. Other column properties are listed in Table 5.2.

5.2. Simulation of 1-column PSA

The initial assessment of the behaviour of a PSA process for CH_4/CO_2 separation was carried out by making simulations of the performance of one column, in a preliminary study. Simulations are quite fast (less than 3 hours, with a processor Intel® Core™ 2 Q9300@2.5 GHz with 4.0 GB of memory) to achieve cyclic steady state (CSS) (more than 85 cycles) and thus it is possible to fix step times to achieve high purity methane. These fast simulations also give us the basic knowledge of the system under study: which are the most important variables, which step or operating variable is the most sensitive one, etc.

An example of the results obtained in 1-column simulation, is depicted in Figure 5.2. The operating conditions of this example are listed Table 5.3. (run 21). The pressure history of this cycle in CSS is shown in Figure 4.2.

Table 5.3. 1-Column PSA performance for CH_4/CO_2 separation using zeolite 13X with modified Skarstrom cycle. Depressurization and equalization time last 25 s.

Run	t_{press} (s)	t_{feed} (s)	t_{blow} (s)	t_{purge} (s)	Q_{purge} (SLPM)	P_{high} (bar)	P_{low} (bar)	*L/D*	CH_4 Purity (%)	CH_4 Recovery (%)	CH_4 Productivity ($mol \cdot kg^{-1} \cdot h^{-1}$)	Power ($kW \cdot mol^{-1}$)
21	50	350	150	250	52.08	4.0	0.3	6.75	99.5	78.7	6.0	0.130

According to the molar flowrate of gases exiting the column it can be observed that desorption of CO_2 in the blowdown step corresponds to almost 50 % while the rest of the CO_2 desorbs in the purge step. This indicates that the purge step is very important in achieving high purity methane. In previous simulations at lower temperature (306 K) (Grande and Rodrigues, 2007a, b), the non-linearity of the CO_2 isotherms is so strong that very small amounts of CO_2 could be desorbed in the purge step. It can be also noted that some CO_2 is exiting the column in the depressurization step. If this stream is recycled, this behaviour should be avoided by reducing the feed time. Also note that the time of the pressure equalization steps was fixed in 25 seconds to accommodate pressure changes without important variations in velocity reducing risks of particle damage by attrition.

The temperature increase (due to adsorption of CO_2) for different positions is also shown in Figure 5.2. When the temperature increases, the loading of CO_2 in the column also decreases considerably (see Figure 5.2c). Another important issue relating the good performance of this

process at 323 K is the amount of CH_4 adsorbed in the column (Figure 5.2d). At lower temperatures, the amount of CH_4 adsorbed in the pressurization step is considerable (around 0.9 $mol \cdot kg^{-1}$) thus requiring larger amounts of CH_4, reducing unit productivity (and product recovery). When temperature increases to 323 K, the amount of CH_4 adsorbed in the pressurization step is less than 0.4 $mol \cdot kg^{-1}$.

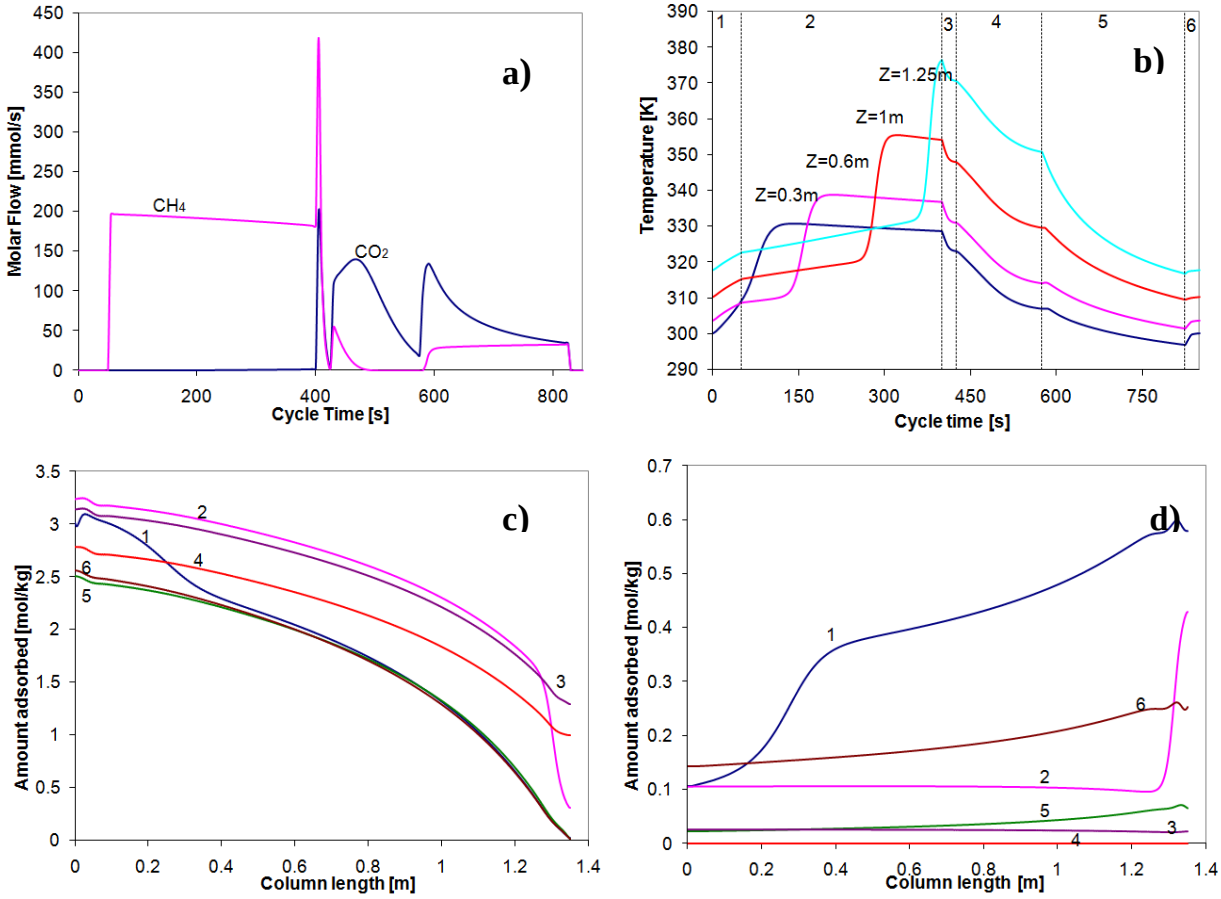

Figure 5.2. 1-column simulation of PSA for CH_4-CO_2 separation using zeolite 13X. Cycle scheme is shown in Figure 4.2 and operating conditions in Table 5.3 (Run 21). Results presented are: a) Molar flowrate of each gas exiting the column, b) temperature histories at different positions (0.3, 0.6, 1 and 1.25 m) from feed inlet, for cyclic steady state, amount adsorbed of c) CO_2 and d) CH_4. Numbers in the figures correspond to the different cycle steps: 1) co-current feed pressurization, 2) adsorption, 3) co-current pressure equalization depressurization, 4) counter-current blowdown, 5) counter-current purge and 6) counter-current pressure equalization pressurization.

Different simulations were performed and the results are summarized in Appendix C, Table C.1. Two important conclusions can be taken from comparison with previous results (Grande and Rodrigues, 2007a, b). Operating at higher temperature resulted in higher product recovery (and thus unit productivity) and also in significant power savings. The low power

consumption is related to the pressure of the blowdown step employed: 0.3 bar instead of 0.1 bar used in previous works (Grande and Rodrigues, 2007a, b).

In these 1-column simulations, the CH_4 purity obtained is quite high. This is a consequence of the operation at higher temperatures: less non linear isotherms and faster diffusion make purge more effective. However, the second reason for this high purity is due to one specification in the simulations: the gas employed in the purge step and pressure equalization is pure methane.

5.3. Effect of recycling streams in PSA

It has been shown that in the simulations of 1-column PSA, product purity around 99 % can be obtained. However, in real systems, recycling a stream with 1 % of CO_2 to the product end will result in higher contamination of the product stream. An apparent solution is to use a partially contaminated stream in the simulations. However, the CO_2 content of these streams should be fixed from the first cycle and may not lead to the correct results. To obtain more realistic results the performance of all the columns should be taken into account.

For a direct comparison of the results of simulating the process with 1 and 2-columns, we will employ the same operating conditions as in run 21 (Table 5.3) and perform the simulation of a 2-column PSA process. The result of the 2-column process simulation is presented in Table 5.4. The pressure history of this cycle is shown in Figure 4.3. Please note that using this cycle, the initial guess for the pressure attained in the depressurization step is the intermediate value between feed and blowdown pressures. This assumption is valid if none of the recycled gases are adsorbed in the zeolite. However, since methane and the small amount of CO_2 recycled are adsorbed the final pressure is lower than this intermediate value. In the molar flowrate of gases exiting the column, there are important differences in the results obtained with simulations of 1-column (Figure 5.2a) and 2-columns (Figure 5.3a). Note that in the CSS of the 2-column simulation, when feed starts, there is some CO_2 exiting the column. This effect results from the recycling of contaminated streams both in purge and in pressure equalization steps. The presence of CO_2 at the end of the column can be observed in Figure 5.3c where more CO_2 is adsorbed at the end of the depressurization step. Also, the amount of CO_2 in the purge does not start from zero since some gas is being recycled and adsorbed in the last layer of adsorbent. The opposite effect is observed in methane loading (Figure 5.3d): less methane is adsorbed since CO_2 is preferably adsorbed. Since we are recycling some CO_2 in the regeneration steps, the temperature increase in the column during the feed step is slightly smaller. In the 2-column simulations,

cyclic steady state is achieved only after 95 cycles: the recycling of CO_2 also added a delay in achieving CSS.

Table 5.4. Comparison between the predicted performance of the studied PSA employing 1-column and 2-columns simulations. All simulations were performed with a purge flowrate of 52.08 SLPM and a feed and blowdown pressures of 4 bar and 0.3 bar, respectively. Pressurization time was 50 s, feed time was 350 s, pressure depressurization and equalization time was 25 s, blowdown time was 150 s and purge time was 250 s.

Run		Q_{feed} (SLPM)	CH_4 Purity (%)	CH_4 Recovery (%)	CH_4 Productivity ($mol \cdot kg^{-1} \cdot h^{-1}$)	Power ($kW \cdot mol^{-1}$)
a	1 Bed	295.12	99.9	72.5	4.7	0.142
	2 Bed	295.12	99.8	83.5	5.4	0.123
b	1 Bed	313.52	99.7	75.1	5.2	0.137
	2 Bed	313.52	99.2	85.0	5.9	0.121
c	1 Bed	329.84	99.6	76.9	5.6	0.133
	2 Bed	329.84	97.9	86.0	6.2	0.120
d	1 Bed	347.2	99.5	78.7	6.0	0.130
	2 Bed	347.2	96.0	86.9	6.6	0.117
e	1 Bed	364.56	99.2	80.1	6.4	0.127
	2 Bed	364.56	94.0	87.6	7.0	0.116
f	1 Bed	373.24	98.5	80.6	6.6	0.126
	2 Bed	373.24	93.0	87.9	7.2	0.115
g	1 Bed	381.92	97.7	81.0	6.8	0.125
	2 Bed	381.92	92.0	88.3	7.4	0.115

It can be observed that when contaminated streams are recycled, the product purity is smaller. However, since we are using a pressure equalization step, there is a significant increase in product recovery (and thus unit productivity). The power consumption per mole is smaller due to the higher productivity; same power consumption with more moles of methane produced.

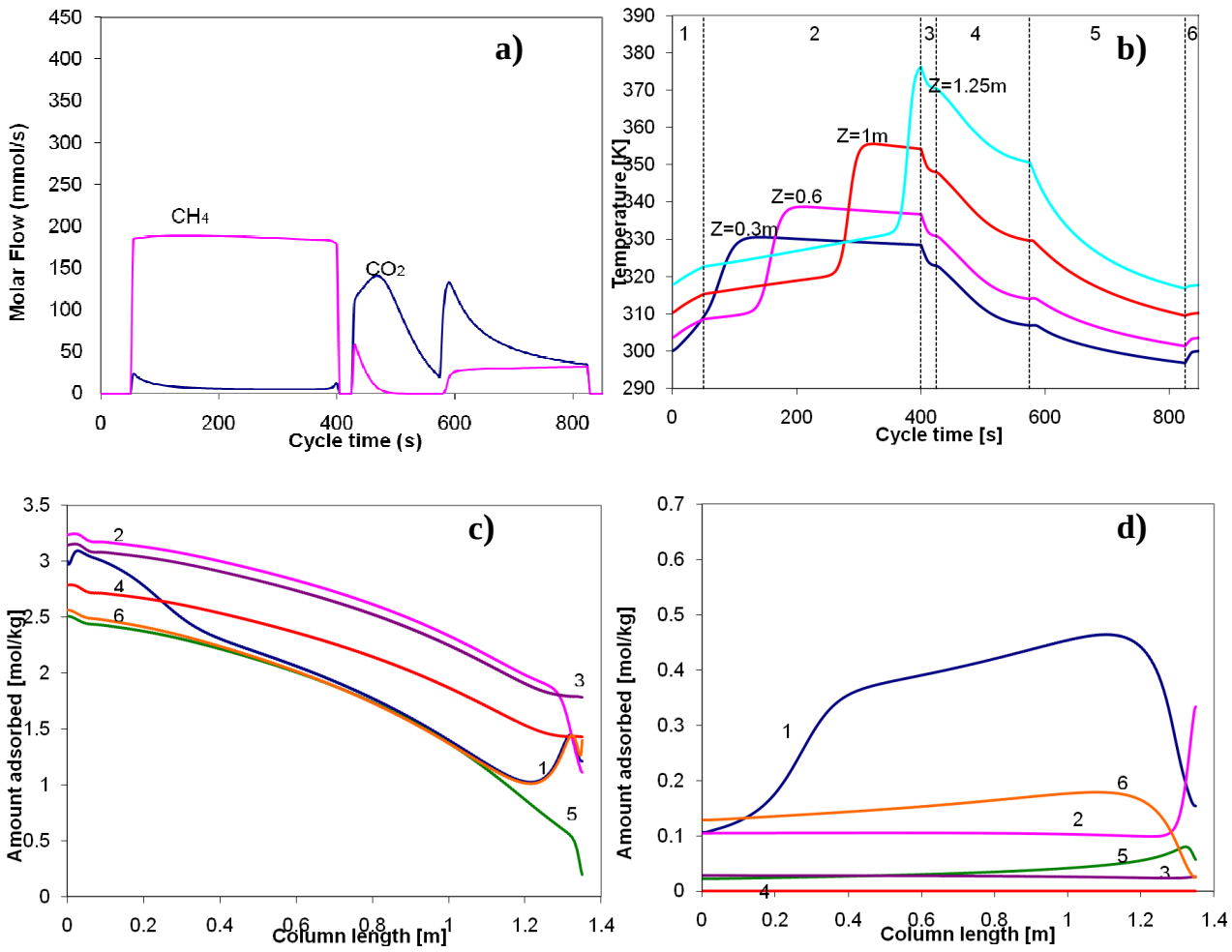

Figure 5.3. 2-column simulation of PSA for CH_4-CO_2 separation using zeolite 13X. Cycle scheme is shown in Figure 4.3 and operating conditions in Table 5.4 (Run d, 2 bed). Results presented are: a) Molar flowrate of each gas exiting the column, b) temperature histories at different positions (0.3, 0.6, 1 and 1.25 m) from feed inlet, for cyclic steady state, amount adsorbed of c) CO_2 and d) CH_4. Numbers in the figures correspond to the different cycle steps: 1) co-current feed pressurization, 2) adsorption, 3) co-current pressure equalization depressurization, 4) counter-current blowdown, 5) counter-current purge and 6) counter-current pressure equalization pressurization.

Finally, the effect of recycling gas streams from one column to the other was evaluated in detail. For this purpose, we have defined all variables in the PSA cycle and vary the amount of feed that the process can admit in the pressurization and feed steps. The results can be observed in Figure 5.4. It is clear that when the methane purity is high (> 99.5 %), simulating a PSA process with 1-column or with 2-columns will result in very similar results of product purity and power consumption. However, when the methane purity decreases to values between 99.5 and 99.0 % larger differences arise from simulating 1-column and the overall process. In this

particular case, if we make simulations of 1-column and obtain a product purity of 98 %, when the process is scaled and more than one column is used, much smaller product purity will be obtained.

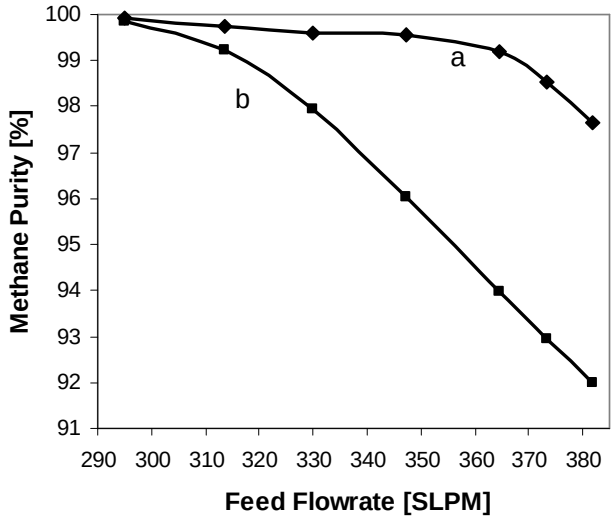

Figure 5.4. Simulation results for PSA cycle employing one and two columns with cycle scheme showed in Figures 4.2 and 4.3, respectively. The simulation conditions are detailed in Table 5.4. Effects in methane purity of feed flowrate for (a) one column (b) two columns.

Simulations of the 2-columns process indicate that CH_4 purity > 99 % can be obtained with product recovery around 85 %. In order to increase the methane recovery, other columns should be employed with further pressure equalization steps.

6. New Cycle Configuration to Enhance Performance of Kinetic PSA Processes

This chapter work deals with the simulation of a new column scheduling for optimized Pressure Swing Adsorption (PSA) operation. The basic information to simulate and design a PSA process, the pure gas adsorption equilibrium and diffusion kinetics in the adsorbent particles, are shown in Chapter 4. The simulation of PSA process was carried out using a mathematical model for a fixed bed described in Chapter 4.

6.1. Cycle design

The final performance of a PSA process to achieve a given separation is dictated by the properties of the adsorbent selected and also by the cycle and operating conditions chosen. In this work, we have evaluated the performance of one new cycle. In order to establish a basis for comparison, all the simulations were carried out using fixed column dimensions (1.35 m of length and 0.1 m of radius) and evaluate the effect of using different feed and purge flowrates.

As mentioned before, the use of lead-trim concept involves a PSA unit with at least three different columns. In order to make the process continuous with a proper schedule, the PSA process simulated is composed by four columns with equal dimensions. Further than testing the lead-trim concept, we have also evaluated the possibility of using less power in the purge step and thus two different cycles were designed.

Note that the use of lead-trim concept involves a stronger interaction between the PSA columns. The column scheme of the lead-trim cycle is presented in Figure 6.1. The cycle is composed by nine different steps:

1. Pressurization: counter-current pressurization with less adsorbed product (CH_4 in this case). The pressure varies from an intermediate pressure (P_{eq}) to the high pressure (P_{high});

2. Trim feed: co-current feed coming from lead column (step 5). The feed stream comes from another bed which means that molar fraction of gases will vary along the duration of this step. In this step, part of the product is removed to be used in the purge step;

3. Feed: co-current feed, where selective removal of heavy gas (CO_2) takes place;

4. Feed 2: co-current feed similar as last step, but the product gas is used for pressurization of another column;

5. Lead-adsorption: in this step, more feed stream is allowed to enter into the column, but the product end is connected to the trim column (step 2) because the heavy gas will break through

the lead column but will be contained with the trim bed. The objective of this step is to exploit more the adsorption capacity of the adsorbent by extending the gas–solid contact time and consequently, to enhance methane productivity;

6. Depressurization: in this step, some gas is allowed to exit the column and be recycled to other column equalizing pressure. It was previously reported that this step results in significant reductions in power consumption (Warmuzinski, 2002);

7. Blowdown: counter-current blowdown where the pressure is reduced to the lower pressure of the cycle. The more adsorbed gas (CO_2) is partially removed from the column in this step;

8. Purge: counter-current purge with less adsorbed gas (CH_4) to displace the heavy gas (CO_2) from the product-end of the column;

9. Equalization: co-current pressure equalization with the gas exiting step 6 from other column to partially increase the pressure of the column. The stream enters from the feed end (co-current) because it is highly contaminated with heavy gas (CO_2).

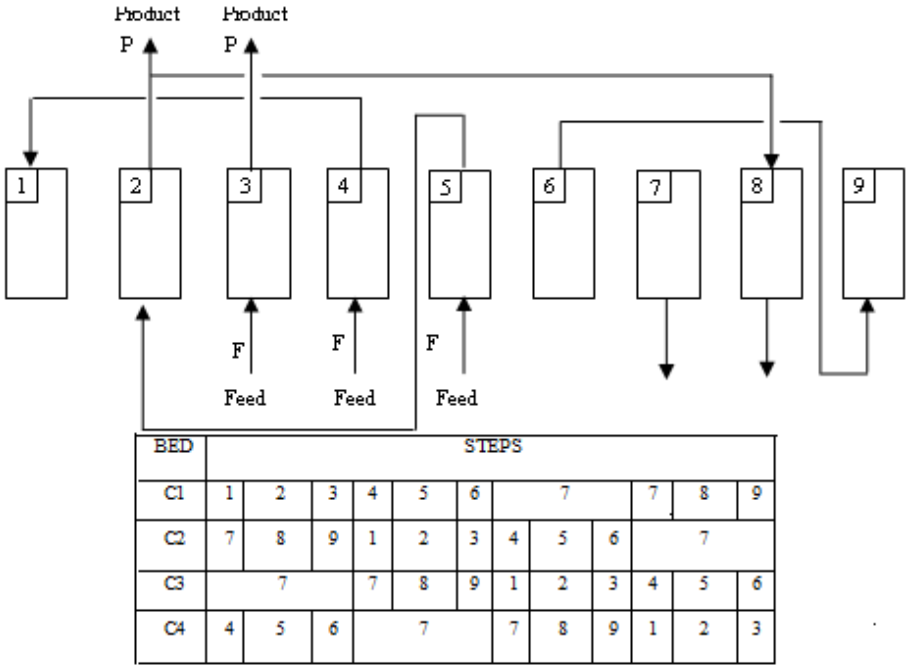

BED	STEPS											
C1	1	2	3	4	5	6	7			7	8	9
C2	7	8	9	1	2	3	4	5	6	7		
C3	7			7	8	9	1	2	3	4	5	6
C4	4	5	6	7			7	8	9	1	2	3

Figure 6.1. PSA cycle scheme used in simulation for PSA Cycle I. Steps are: 1) counter-current product pressurization, 2) trim feed, 3) feed, 4) feed 2, 5) lead adsorption, 6) co-current pressure equalization depressurization, 7) counter-current blowdown, 8) counter-current purge with product and 9) co-current pressure equalization pressurization.

Note that this cycle also integrates the pressure equalization in a non-standard way. It should be noted that the stream leaving the depressurization step is highly contaminated with CO_2 and if it is not recycled, important amounts of methane will be lost in the blowdown step.

The PSA performance is measured by four interrelated parameters: product purity and recovery, unit productivity and power consumption. These performance variables are somewhat different those defined in Chapter 4 because the cycle configuration is also different.

Product (CH_4) purity is defined for the stream exiting the trim bed and feed steps by:

$$Purity = \frac{\int_0^{t_{feed}} C_{CH_4} u\big|_{Z=Lc} dt + \int_0^{t_{trim}} C_{CH_4} u\big|_{Z=Lc} dt}{\left(\int_0^{t_{feed}} C_{CH_4} u\big|_{Z=Lc} dt + \int_0^{t_{feed}} C_{CO_2} u\big|_{Z=Lc} dt + \int_0^{t_{trim}} C_{CH_4} u\big|_{Z=Lc} dt + \int_0^{t_{trim}} C_{CO_2} u\big|_{Z=Lc} dt \right)} \quad (6.1)$$

The CH_4 recovery, calculated by equation 6.2, is defined by the ratio between the number of moles of methane obtained as product divided by the number of moles of CH_4 introduced in the feed and lead feed steps.

$$\text{Recovery} = \frac{\left(\int_0^{t_{feed}} C_{CH_4} u\big|_{Z=Lc} dt + \int_0^{t_{trim}} C_{CH_4} u\big|_{Z=Lc} dt \right) - \int_0^{t_{purge}} C_{CH_4} u\big|_{Z=Lc} dt}{\int_0^{t_{feed}} C_{CH_4} u\big|_{Z=0} dt + \int_0^{t_{lead}} C_{CH_4} u\big|_{Z=0} dt} \quad (6.2)$$

The CH_4 productivity is measured by the amount of product processed per unit amount of adsorbent per unit time. It is calculated by:

$$\text{Productivity} = \frac{y_{feed,CH_4} \dot{n}_{feed} \text{Recovery}}{t_{total} w_{ads}} \quad (6.3)$$

where t_{total} is the total cycle time, $\dot{n}_{feed}$ is the number of moles of biogas fed to the column in the feed, y_{feed,CH_4} is the molar fraction of methane in the feed stream and lead steps and w_{ads} the adsorbent mass.

The power consumption is defined as the required energy for compression of the different streams and the energy requirements of the PSA unit; it is calculated by adiabatic compression given in Chapter 4, equation 4.14.

6.2. Results and Discussion

The PSA simulations were performed for the two different PSA Cycle configurations and the two adsorbents under study, zeolite 13X and CMS-3K. To establish a comparison basis, all experiments were performed with the same feed operating conditions (P, T, composition)

varying the inlet flowrate for the different cases. Blowdown pressure was also fixed since this parameter will introduce large variations in process performance. The column properties and the operating conditions, as well as the zeolite 13X properties, used in the PSA simulations were already detailed in Chapter 5, Tables 5.2 and 5.1, respectively. The CMS-3K physical properties are shown in Table 6.1. The beds were also assumed to be initially filled with helium, which is considered to be a non-adsorbed gas at present temperature and pressure.

Table 6.1. Physical properties of the CMS-3K employed in the PSA simulations. The tortuosity was assumed constant and equal to 2.0.

Adsorbent	CMS-3K
Column porosity	0.33
Column density ($kg \cdot m^{-3}$)	715.0
Pellet density ($kg \cdot m^{-3}$)	1,060
Pellet porosity	0.46
Pellet radius (m)	0.0009
Mean pore radius (A)	1,560
Specific heat ($J \cdot kg^{-1} \cdot K^{-1}$)	880

Before reporting the results obtained with the new cycles studied in this work it is proper to give some details of the PSA performance obtained with those adsorbents using a Skarstrom cycle (comprising pressurization, feed, depressurization, blowdown, purge and pressure equalization). Using zeolite 13X, the process is strongly controlled by energy transfer (Cavenati et al., 2006b). The amount of CO_2 adsorbed per kilogram of zeolite is enough to generate large amounts of heat that contribute to large temperature variations inside the column resulting in dispersion of the concentration waves. Also, the regeneration of the adsorbent is quite difficult since the adsorption isotherms of CO_2 are quite steep. For this reason, increasing the temperature from 300 K to 323 K has resulted in better operation with much higher unit productivities. Previous studies employing this adsorbent showed that methane purity over 98 % can be obtained with a unit productivity of 3.83 mol $CH_4 \cdot kg^{-1} \cdot h^{-1}$ (Grande and Rodrigues, 2007a). These results indicate that is possible an improvement in the methane productivity for 5.5 mol $CH_4 \cdot kg^{-1} \cdot h^{-1}$ with the same purity product.

On the other side, when the adsorbent selected is CMS-3K, the process is entirely dominated by mass transfer into the micropores of the adsorbent (Farooq et al., 2002). The

amount of methane adsorbed per cycle is extremely small and it can be assumed that the methane that can penetrate the micropores cannot be desorbed under normal operation. It can be observed that during cyclic steady state no methane is adsorbed per cycle (Cavenati et al., 2005). However, the diffusion coefficient of CO_2 is also small and the MTZ of CO_2 is also widespread along the column. Thermal variations within the column do exist in this case, but are of secondary importance when compared to mass transfer. The regeneration of the adsorbent is also difficult since the adsorbed CO_2 cannot be displaced by CH_4 once that this gas does not penetrate into the micropores. It was also verified that at ambient temperature the performance of CMS-3K is better than the zeolite 13X (Grande and Rodrigues, 2007a). We have also verified that increasing the temperature to 323 K it was possible to increase the regeneration pressure to 0.3 bar and also improve process performance: in zeolite 13X the isotherms are less steep (Santos et al., 2010) and in CMS-3K the CO_2 diffusion rate increases.

The modified cycles intend to improve the process performance by enhancing contact time between gas and adsorbent.

6.2.1. Cycle I: 9-step lead-trim operation

When using a kinetic adsorbent like CMS-3K for CH_4-CO_2 separation, the diffusion rate of methane is extremely slow, but the diffusion rate of CO_2 is also slow. This slow CO_2 diffusion rate results in a large mass transfer zone (MTZ) within the column. When large MTZ exists, the feed step should be stopped prematurely, before a significant loading of the bed can be achieved. This means that a large portion of the adsorbent within the column is not effectively used for bulk separation, reducing the productivity of the process. For this kind of kinetic processes, we have employed an alternative column arrangement for an enhanced utilization of the adsorbent within the columns. In this new column arrangement, when the concentration front of CO_2 is near the product end, the column is connected to other column and still processing the feed stream. With this connection, more time for diffusion is provided to the adsorbent within the first column before column regeneration. This temporary enhancement of column length in the lead-trim approach intends to overcome problems of MTZ with kinetic adsorbents without using columns with double the length where the MTZ problem will still be present.

Potentially, this cycle can be employed to all PSA processes using kinetic-driven adsorbents improving the process productivity. Moreover, the cycle can be employed to PSA processes where loading is severely affected by temperature variations. In fact, in these cycles, the effective loading of the adsorbent is reduced because of temperature increase of the

adsorbent. If more time is allowed for contacting with the "cold" feed stream, more loading can be used, improving the process performance. The aim of this chapter is to describe the results obtained for these two different approaches using this cycle. The cycle displayed in Figure 6.1 was used for the simulations. The results presented here result from the simulation of a four-column PSA unit. In all the simulations performed with this cycle the purge flow rate, the total cycle time and the feeding time (trim-feed, feed and lead-feed) were assumed constants.

The results obtained for CMS-3K are presented in Table 6.2 while results for zeolite 13X are listed in Table 6.3. The results shown in these tables can be better understood by observing the behaviour of the two different systems.

6.2.1.1. CMS-3K adsorbent

In Figure 6.2 the pressure history and the molar flowrate exiting the column are shown (run i in Table 6.2) at Cyclic Steady State (CSS). The CSS is reached after 40 cycles. It can be observed that although CO_2 starts to break through the column trim-column at the end of the lead-feed, overall product purity is higher than 98 %. In this image it can be observed that there is some CO_2 exiting the column even in the initial seconds of the feed, because the stream used in the purge step is not pure methane but contaminated gas recycled from other steps. It can also be observed that the stream exiting the depressurization step has important amounts of CO_2 and thus it should be recycled by the feed end to avoid contamination of the product end.

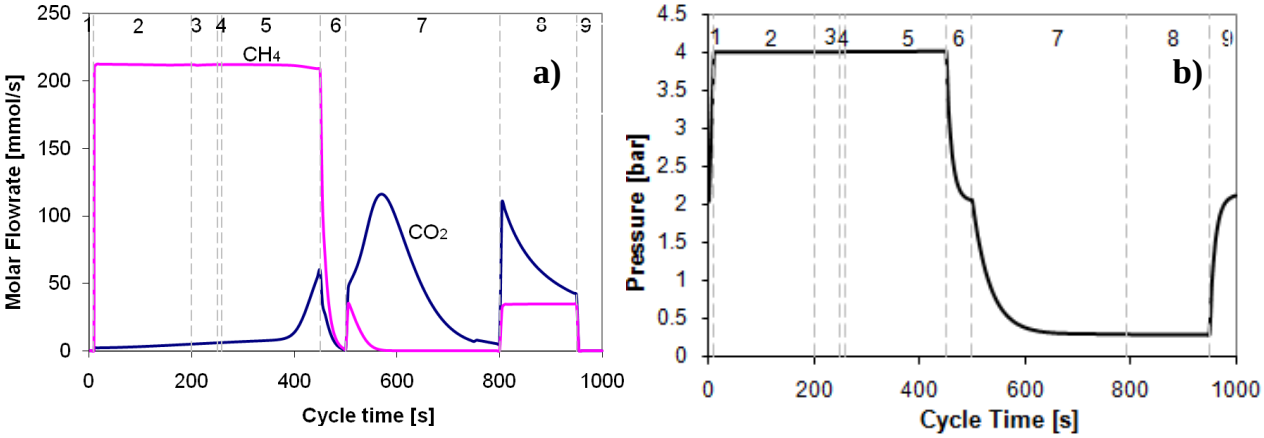

Figure 6.2. 4-column simulation of PSA for CH_4-CO_2 separation using CMS-3K. Cycle scheme is shown in Figure 6.1 and operating conditions in Table 6.2 (Run i). Results presented are: a) molar flowrate of each gas exiting the column and b) and typical pressure history of one CSS cycle used in simulation for PSA Cycle I. Numbers in the figures correspond to the different cycle steps: 1) counter-current product pressurization, 2) trim feed, 3) feed, 4) feed 2, 5) lead adsorption, 6) co-current pressure equalization depressurization, 7) counter-current blowdown, 8) counter-current purge with product and 9) co-current pressure equalization pressurization.

In Figure 6.3 the internal CO_2 concentration profiles at the end of each step are shown. Also, the amount adsorbed of both CO_2 and CH_4 are displayed together with the temperature evolution in different positions of the column. It can be observed that temperature variations are considerable in the whole column (up to 20 K). It can also be observed that the amount of methane adsorbed in cyclic steady state is also extremely small running at 323 K.

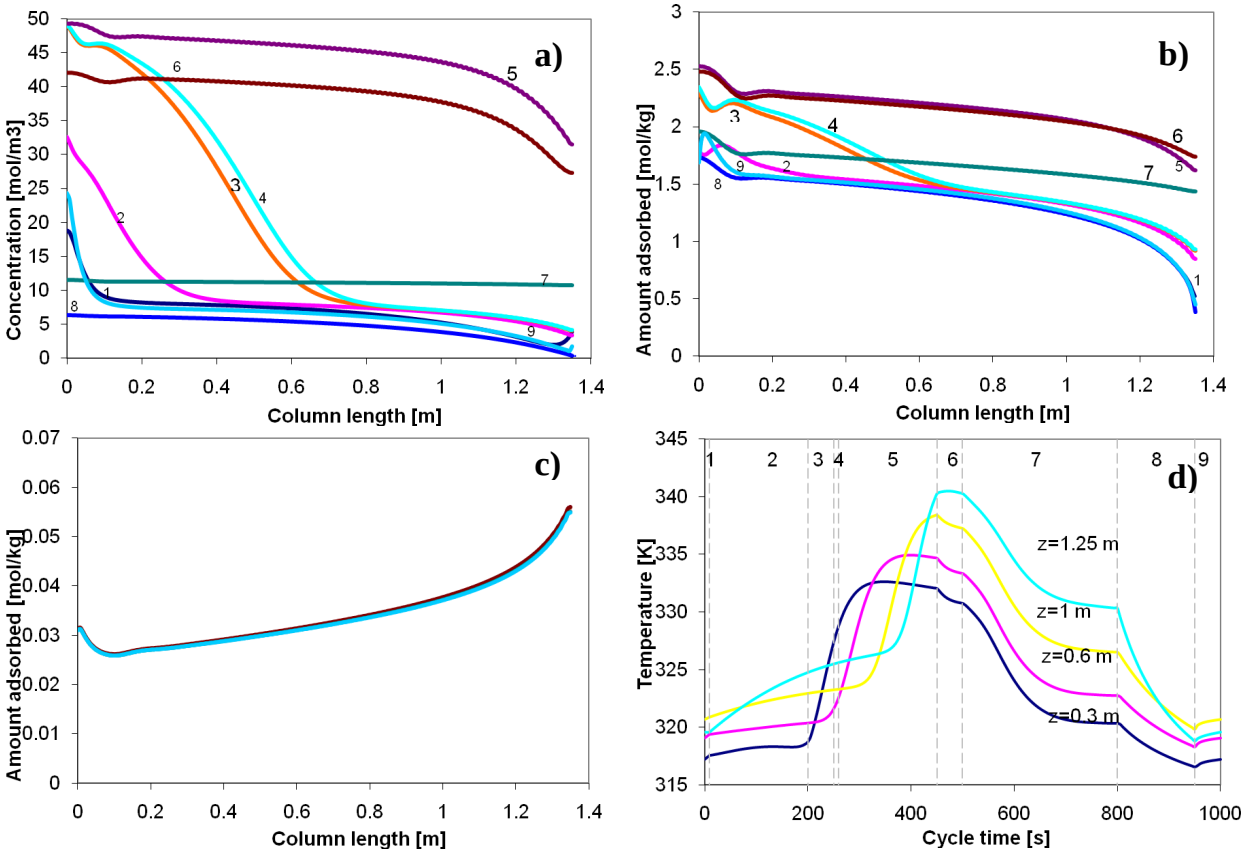

Figure 6.3. 4-column simulation of PSA for CH_4-CO_2 separation using CMS-3K. Cycle scheme is shown in Figure 6.1 and operating conditions in Table 6.2 (Run i). Results presented are: a) gas phase concentration of CO_2, b) amount adsorbed of CO_2, c) amount adsorbed of CH_4 and d) steady state temperature profiles at different positions (0.3, 0.6, 1 and 1.25 m) from feed inlet. Numbers in the figures correspond to the different cycle steps: 1) counter-current product pressurization, 2) trim feed, 3) feed, 4) feed 2, 5) lead adsorption, 6) co-current pressure equalization depressurization, 7) counter-current blowdown, 8) counter-current purge with product and 9) co-current pressure equalization pressurization.

The benefits of the lead-trim cycle can be observed in the amount of CO_2 adsorbed and in the gas phase at the end of the trim feed step (step 2) and at the end of the lead feed step (step 5). It can be observed that at the end of the trim feed, the amount of CO_2 adsorbed is considerable only in the initial portion of the bed. This is in agreement with previous results using this adsorbent (Grande and Rodrigues, 2007a). This zone is followed by a large MTZ which corresponds to more than 50 % of the column. Using a lead-trim cycle, more feed is allowed to

the column, the CO_2 concentration front is moving along the column (from step 2 to step 4), using almost 50 % of the bed and adsorbing much more CO_2.

It can be observed in Table 6.2 that the initial flowrate employed is 347.2 SLPM (standard litters per minute). This flowrate was increased more than 30 % (up to 451.4 SLPM) keeping purity over 98 %. In fact, the increase of feed flowrate is reflected in the unit productivity of the system that has increased from 4.0 to 5.5 mol CH_4 produced per kilogram of adsorbent per hour. The recovery of this cycle is also high (88.5%) with a very small slip-off of CH_4 in the blowdown step. The improvement in unit productivity is also reflected in the power consumption of the system: since more methane is produced, less energy is spend in the separation. 55 % of this energy is spent for compression the product up to 200 bar.

Table 6.2. 4-Column PSA performance for CH_4/CO_2 separation using CMS-3K and the first cycle configuration. All simulations were performed with a purge flowrate of 52.08 SLPM and a feed and blowdown pressures of 4 bar and 0.3 bar, respectively. Equalization and feed times were 50 s, blowdown time was 300 s, purge time was 150 s and lead time was 200 s

Run	t_{press}	t_{trim}	Q_{feed} (SLPM)	CH_4 Purity (%)	CH_4 Recovery (%)	CH_4 Productivity ($mol \cdot kg^{-1} \cdot h^{-1}$)	Total Power ($kW \cdot mol^{-1}$) *	Cycle Power ($kW \cdot mol^{-1}$)
f	12	188	347.2	99.4	83.9	4.0	0.170	0.0785
g	10	190	416.64	98.5	87.6	5.0	0.166	0.0749
h	10	190	434	98.3	87.6	5.2	0.166	0.0747
i	9	191	451.36	98.3	88.5	5.5	0.165	0.0740
j	9	191	468.72	97.9	88.9	5.7	0.165	0.0739

* Total power comprises the cycle power consumption and the power spent in product compression.

6.2.1.2 Zeolite 13X adsorbent

The results obtained from the PSA simulations using zeolite 13X are somewhat different, for example, the CSS is reached only after 70 cycles. The molar flowrate exiting the column and the temperature evolution per cycle in different positions of the column can be observed in Figure 6.4 for run e described in Table 6.3.

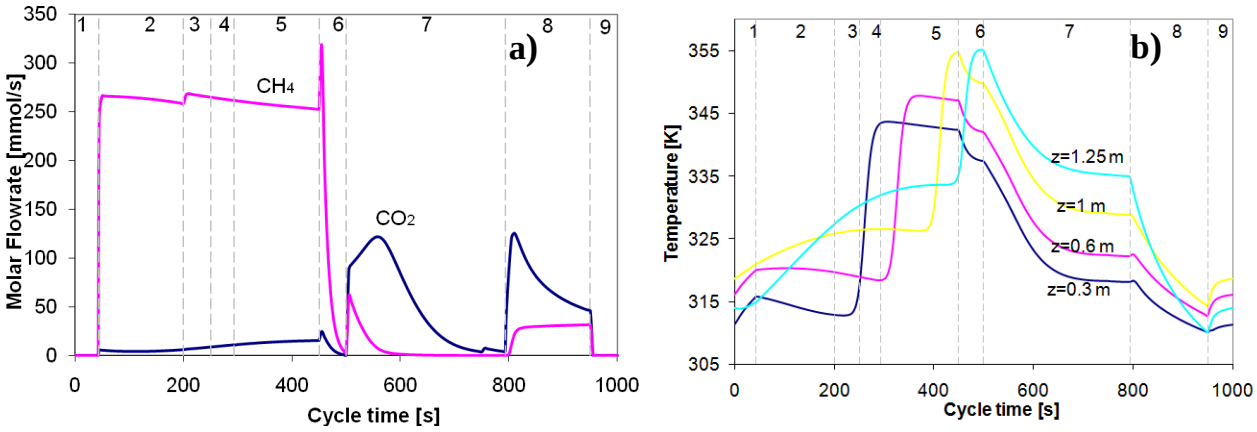

Figure 6.4. 4-column simulation of PSA for CH_4-CO_2 separation using Zeolite 13X. Cycle scheme is shown in Figure 6.1 and operating conditions in Table 6.3 (Run e). Results presented are: a) molar flowrate of each gas exiting the column and b) steady state temperature profiles at different positions (0.3, 0.6, 1 and 1.25 m) from feed inlet. Numbers in the figures correspond to the different cycle steps: 1) counter-current product pressurization, 2) trim feed, 3) feed, 4) feed 2, 5) lead adsorption, 6) co-current pressure equalization depressurization, 7) counter-current blowdown, 8) counter-current purge with product and 9) co-current pressure equalization pressurization.

Table 6.3. 4-Column PSA performance for CH_4/CO_2 separation using Zeolite 13X and the first cycle configuration. All simulations were performed with a purge flowrate of 52.08 SLPM and a feed and blowdown pressures of 4 bar and 0.3 bar, respectively. Equalization and feed times were 50 s and the lead time was 200 s

Run	t_{press}	t_{trim}	t_{blow}	t_{purge}	Q_{feed} (SLPM)	CH_4 Purity (%)	CH_4 Recovery (%)	CH_4 Productivity ($mol \cdot kg^{-1} \cdot h^{-1}$)	Total Power ($kW \cdot mol^{-1}$) *	Cycle Power ($kW \cdot mol^{-1}$)
a	60	140	310	140	347.2	99.3	77.9	3.2	0.191	0.0819
b	46	154	296	154	434	98.8	86.1	4.4	0.180	0.0700
c	45	155	295	155	451.36	98.6	86.9	4.6	0.179	0.0689
d	44	156	294	156	468.72	98.4	87.6	4.8	0.178	0.0678
e	43	157	293	157	486.08	98.0	88.2	5.0	0.173	0.0668

* Total power comprises the cycle power consumption and the power spent in product compression.

In this example, temperature oscillations of 40 K are observed which result in strong variations of CO_2 adsorbed inside the column. In this cycle, also CO_2 does not break through the column and again contamination of CO_2 is due to recycling of dirty stream in the purge and pressurization steps. However, in this example, two important differences can be observed. In this adsorbent, methane adsorption and desorption cannot be neglected and thus more methane is

lost in the blowdown step and is also employed in the pressurization step. For this reason, it can be observed in Table 6.3 that more feed is processed using this adsorbent, but unit productivity is smaller. The CO_2 concentration in gas phase and CH_4 and CO_2 adsorbed at the end of each step are also shown in Figure 6.5. The MTZ due to mass transfer and due to thermal effects can be clearly identified for this example. In this Figure it can also be observed that considerable amount of methane is employed in pressurization and is also released in the blowdown step.

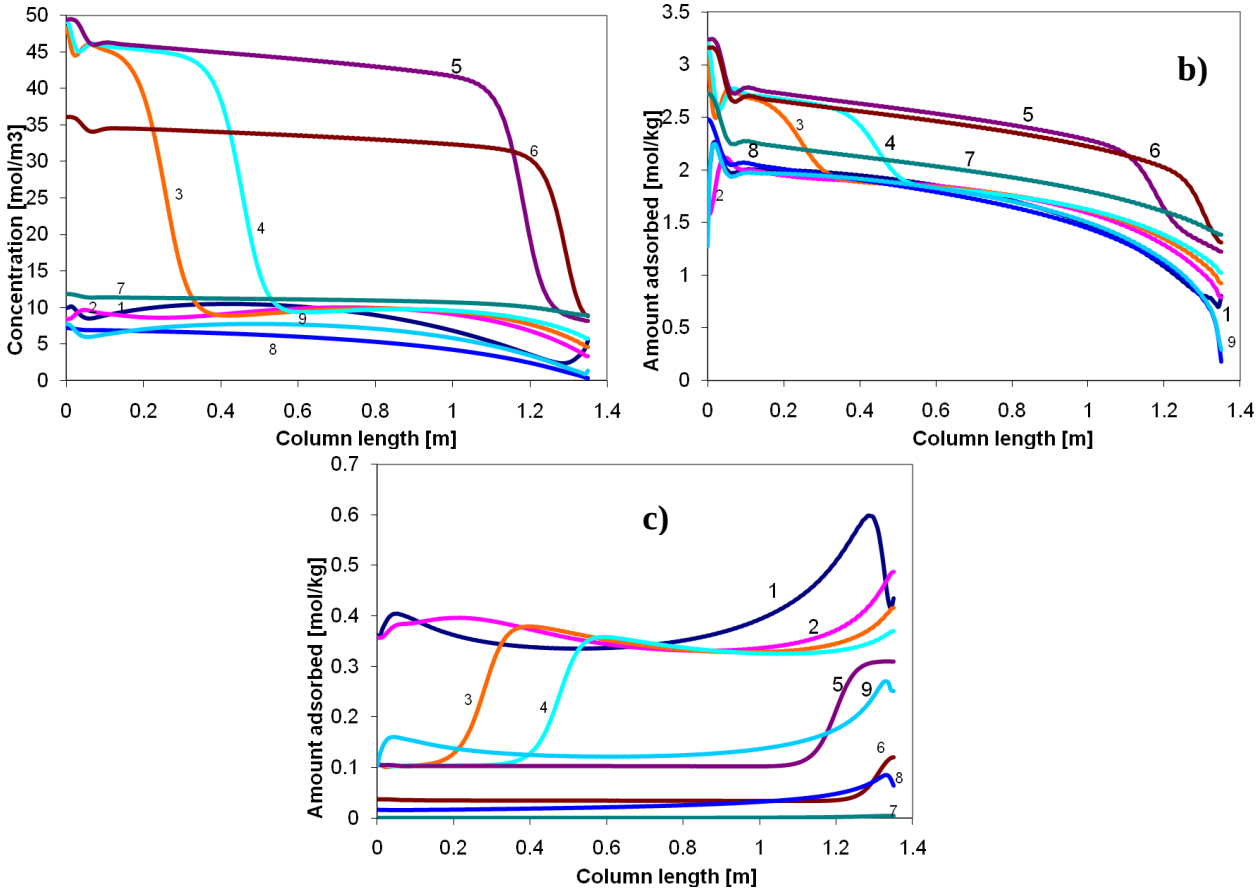

Figure 6.5. 4-column simulation of PSA for CH_4-CO_2 separation using Zeolite 13X. Cycle scheme is shown in Figure 6.1 and operating conditions in Table 6.3 (Run e). Results presented are: a) gas phase concentration of CO_2, b) amount adsorbed of CO_2 and c) amount adsorbed of CH_4. Numbers in the figures correspond to the different cycle steps: 1) counter-current product pressurization, 2) trim feed, 3) feed, 4) feed 2, 5) lead adsorption, 6) co-current pressure equalization depressurization, 7) counter-current blowdown, 8) counter-current purge with product and 9) co-current pressure equalization pressurization.

Despite the poorer results obtained with the zeolite 13X, it was demonstrated that the lead-trim concept can also be employed in adsorbents with faster diffusion kinetics. The major problems in these adsorbents are the thermal variations along one cycle that cannot be overcame with the lead-trim arrangement.

7. Conclusions and Recommendation for Future Work

7.1. Conclusions

In this work, the simulations of a Pressure Swing Adsorption process for biogas upgrading (CH_4-CO_2 separation) were carried out using zeolite 13X and CMS-3K as selective adsorbent.

In the first part of this work, a 6-step PSA cycle comprising pressurization, feed, depressurization, blowdown, purge and pressure equalization employing the zeolite 13X as adsorbent was studied. It was demonstrated that operating at 323 K is beneficial for this adsorbent because adsorption equilibrium isotherm is not very steep (like at 299 K) and thus regeneration can be carried out at mild pressures and purge can remove more CO_2. Unit productivity around 6 $mol \cdot kg^{-1} \cdot h^{-1}$ was obtained with a power consumption of 0.12 $kW \cdot mol^{-1}$ CH_4 produced.

The simulation of a two-column PSA process was also assessed. It was observed that when streams with more than 0.5 % of CO_2 are recycled in the purge and pressure equalization steps, there is a severe decrease in the methane purity obtained as product. The important benefit of using pressure equalization relies in the increase of product recovery which is always higher than 80 %. With these two-column process simulations it was possible to find conditions to operate the PSA and produce methane with purity of 99.2 %, recovery of 85.0 % with a unit productivity of 5.9 mol $CH_4 \cdot kg^{-1} \cdot h^{-1}$ and a power consumption of 0.12 $kW \cdot mol^{-1}$ CH_4 produced. This result is much more realistic than the one obtained with simulations of 1-column that should only be considered as accurate if high purity gases are recycled in purge and pressure equalization steps.

After that, the simulation of a new PSA cycle using lead-trim concept was studied. The new concept was presented for the two adsorbents already referred. These adsorbents are characterized by slow and fast kinetics where mass transfer zone is dominated either by mass transfer or by thermal variations. The simulations were carried out to separate a stream of 67 % of CH_4 and 33 % of CO_2 in order to obtain CH_4 with purity over 98 %. The lead-trim concept used here involves a deeper interaction between the PSA columns and nine-step cycle in a four-column PSA was used for simulations. The results indicate that it was possible to obtain high purity methane (purity over 98 %) with both adsorbents.

For the case of CMS-3K (slow kinetic adsorbent), the utilization of the bed has drastically increased when compared to a classical PSA unit. The use of a lead-trim concept allow the adsorbent to process much more feed than in classical operation allowing better unit

productivities and also very small amounts of methane are lost in the blowdown step (methane recovery over 88 %). The unit productivity is as high as 5.5 mol $CH_4 \cdot kg^{-1} \cdot h^{-1}$ and power consumption is 0.074 $kW \cdot mol^{-1}$ CH_4 produced.

When zeolite 13X is used, the lead-trim concept is also successful in improving the unit productivity, but in this case the improvement is smaller. Using zeolite 13X, the temperature variations due to CO_2 adsorption and desorption are intense and will have a large influence in the final PSA performance. Also, using zeolite 13X, the methane adsorption in pressurization step is important resulting in a smaller production of methane from feed step.

The lead-trim concept can be employed in kinetic-controlled PSA units as well as equilibrium-controlled ones. It is expected however that the improvements in the case of equilibrium-controlled PSA are smaller than in the case of kinetic-controlled PSA operations. For kinetic-controlled PSA units, this kind of column operation may result in further reduction of PSA size and also have some impacts in reducing power consumption.

7.2. Objectives Achieved and Recommendation for Future Work

The upgrading of biogas to obtain bio-methane (purity > 98 %), that can be used as renewable fuel, was successfully studied by PSA process. It was found that the recycle of streams with purity lower than 99 % results in a significant decrease in the overall purity of bio-methane. It was also concluded that the lead-trim concept can be employed in kinetic-controlled PSA units as well as equilibrium-controlled ones.

It can be concluded that the PSA process is a successful mean in the biogas separation but have some limitations in the operation conditions like, temperature and pressure, which it is reflected in the operation costs. It was verified with this work that the temperature increase and the regeneration step may be performed at higher pressure (0.3 instead of 0.1 bar) than that used in LSRE previous studies. Therefore, it is recommend more studies to optimize this process for biogas separation and two overcome the thermal effects of equilibrium adsorbents.

References

Air Liquide. Medal™ membrane technology; http://www.medal.airliquide.com/en/co-membrane/co-membrane-technology.html (accessed March 2010).

Anson, A.; Lin, C. C. H.; Kuznicki, S. M.; Sawada, J. A. 2009. Adsorption of carbon dioxide, ethane, and methane on titanosilicate type molecular sieves, Chem. Eng. Sci., 64, 3683–3687.

Basmadjian, D. 1997. The Little Adsorption Book: A Practical Guide for Engineers and Scientists; CRC Press.

Berlin, N.H.1966. Method for providing an oxygen-enriched environment. U.S.Patent 3,280,536.

Bird, R.B., Stewart, W.E., and Lightfoot, E.N. 2002. Transport Phenomena; 2nd Edn; Wiley International: Singapore.

Bonnot, K.; Tondeur, D. 2006. Effects of Composition, Temperature and Purge on the Performance of the Cyclic Adsorption of CO_2 and CH_4 on Activated Carbon. Chemical Engineering Research and Design, 84(A3), 192-208.

CarboTech. Carbon molecular sieves flyer; http://www.carbotech.de/pdf_viewer/pdf_view.php?pdf_file=carbotech_cms_folder_en.pdf (accessed March 2010).

Cavenati, S.; Grande, C. A.; Rodrigues, A. E. 2005. Upgrade of Methane from Landfill Gas by Pressure Swing Adsorption. Energy Fuels, 19, 2545-2555.

Cavenati, S.; Grande, C.A.; Rodrigues, A.E.2006.Separation of $CH_4/CO_2/N_2$ mixtures by layered Pressure Swing Adsorption for upgrade of natural gas. Chem. Eng. Sci., 61, 3893-3906. **(a)**

Cavenati, S., Grande, C. A., Rodrigues, A. E., 2006. Removal of Carbon Dioxide from Natural Gas by Vacuum Pressure Swing Adsorption. Energy & Fuels, 20, 2648-2659. **(b)**

Cavenati, S.; Grande, C. A.; Rodrigues, A. E. 2008. Metal Organic Framework Adsorbent for Biogas Upgrading, Ind. Eng. Chem. Res., 47, 6333-6335.

Cavenati, S., Grande, C. A., Lopes, F.V.S., Rodrigues, A.E., 2009. Adsorption of small molecules on alkali-earth modified titanosilicates. Microporous and Mesoporous Materials, 121, 114-120.

Chagger, H.K., Ndaji, F. E., Sykes, M. L., Thomas, K. M., 1995. Kinetics of adsorption and diffusional characteristics of carbon molecular sieves. Carbon, 33, 1405-1411.

Chen, Y. D.; Yang, R. T.; Uawithya, P. 1994. Diffusion of Oxygen, Nitrogen and Their Mixtures in Carbon Molecular Sieve. AIChE J., 44, 577.

Da Silva, F. A., Silva, J. A., Rodrigues, A. E. 1999. A General Package for the Simulation of Cyclic Adsorption Processes. Adsorption, 5, 229-244.

Da Silva, F. A., Rodrigues, A. E. 2001. Propylene/Propane Separation by Vacuum Swing Adsorption Using 13X Zeolite. AIChE J., 47, 341-357.

Davis, M. M.; Gray, R. L. J.; Patei, K. 1992. Process for the Purification of Natural Gas. US Patent, No 5174796.

Delgado, J.A.; Uguina, M.A.; Sotelo, J.L.; Ruíz, B.; Gómez, J.M. 2006. Fixed-bed adsorption of carbon dioxide/methane mixtures on silicalite pellets. Adsorption, 12, 5-18. **(a)**

Delgado, J.A.; Uguina, M.A.; Sotelo, J.L.; Ruíz, B.; Rosário, M. 2006. Separation of carbon dioxide/methane mixtures by adsorption on a basic resin. Adsorption, 13, 373-383. **(b)**

Delgado, J.A.; Uguina, M.A.; Sotelo, J.L.; Ruíz, B.; Rosário, M. 2007. Carbon Dioxide/Methane Separation by Adsorption on Sepiolite. Journal of Natural Gas Chemistry, 16, 235-243.

Delgado, J. A.; Rodrigues, A. E. 2008. Analysis of the Boundary Conditions for the simulation of the Pressure equalization Step in PSA cycles, Ind. Eng. Chem. Res., 63, 4452-4463.

Do, Doung D. 1998. Adsorption Analysis: Equilibria and Kinetics, Vol2, Imperial College Press.

Dolan, W. B.; Mitariten, M. J. 2003. CO_2 Rejection from Natural Gas. US Patent, No 2003/0047071. **(a)**

Dolan, W. B.; Mitariten, M. J. 2003. Heavy Hydrocarbon Recovery from Pressure Swing Adsorption Unit Tail Gas. US Patent, No 6,610,124. **(b)**

Dominguez, J. A.; Psaras, D.; LaCava, A. I. 1988. Langmuir Kinetics as an Accurate Simulation of the Rate of Adsorption of Oxygen and Nitrogen Mixtures on Non-Fickian Carbon Molecular Sieves. AIChE Symp. Ser., 84, 73.

Farooq, S., Qinglin, H., Karimi, I. A., 2002. Identification of transport mechanism in adsorbent micropores from column dynamics. Ind. Eng. Chem. Res., 41, 1098-1106.

Fitch, F. R.; Bulow, M.; LaCava, A. I. 1994. Investigation of the Mechanism for the Separation of Nitrogen-Oxygen Mixtures on Carbon Molecular Sieves. Gas Sep. Purif., 8, 45.

Foundation for Biotechnology Awareness and Education (FBAE); http://fbae.org/2009/FBAE/website/our-position-biofuel_potential-future-crop-of-farmers.html (accessed March 2010).

Fujita, S.; Himeno, S.; Suzuki, K. 2006. Method for Concentrating Methane from Sewage Sludge and Methane Storage Equipment. European Patent, EP 1,647,531, Al.

GHG Data; United Nations Framework Convention on Climate Change; http://unfccc.int/ghg_data/ghg_data_unfccc/items/4146.php (accessed March 2010).

Gomes, V.G.; Hassan, M.M. 2001. Coalseam methane recovery by vacuum swing adsorption, Sep. Purif. Technol., 24, 189–196.

Grande, C. A.; Silva, V. M. T. M.; Gigola, C.; Rodrigues, A. E. 2003. Adsorption of Propane and Propylene onto Carbon Molecular Sieve. Carbon, 41, 2533-2545.

Grande, C.A.; Rodrigues, A.E. 2007. Biogas to Fuel by Vacuum Pressure Swing Adsorption I. Behavior of Equilibrium and Kinetic Adsorbents. Ind. Eng. Chem. Res., 46, 4595-4605. **(a)**

Grande, C.A.; Rodrigues, A.E. 2007. Layered Vacuum Pressure- Swing Adsorption for Biogas Upgrading. Ind. Eng. Chem. Res., 46, 7844-7848. **(b)**

Hagen, M., Polman, E., Jensen, J. K., Myken, A., Jönsson, O.; Dahl, A., 2001. Adding gas from biomass to the gas grid. Report SGC 118, Swedish Gas Centre.

Jacobsson, E. 2009. Upgrading biogas to natural gas quality. European Biomethane Fuel Conference. Göteborg, Sweden, September 7-9.

Jayaraman, A.; Hernandez-Maldonado, A. J.; Yang, R. T.; Chinn, D.; Munson, C. L.; Mohr, D. H. 2004. Clinoptilolites for nitrogen/methane separation. Chem. Eng. Sci., 59, 2407-2417.

Jayaraman, A.; Yang, R. T.; Chinn, D.; Munson, C. L. 2005. Tailored Clinoptilolites for Nitrogen/Methane Separation. Ind. Eng. Chem. Res., 44, 5184-5192.

Jüntgen, H.; Knoblauch, K.; Harder, K.1981. Carbon Molecular Sieves: Production from Coal and Applications in Gas Separation. Fuel, 60, 817-822.

Kapoor, A.; Yang, R.T. 1989. Kinetic Separation of Methane - Carbon Dioxide Mixture by Adsorption on Molecular Sieve Carbon. Chem. Eng. Sci., 44, 1723–1733.

Keller, G. E., Anderson, R. A., Yon, C. M., 1987. Handbook of Separation Process Technology. JohnWiley, New York.

Kim, M.-B.; Bae, Y.-S.; Choi, D. K.; Lee, C.-H. 2006. Kinetic Separation of Landfill Gas by a Two Bed Pressure Swing Adsorption Process Packed with Carbon Molecular Sieve: Nonisothermal Operation. Ind. Eng. Chem. Res., 45, 5050.

Knaebel, K.S.; Reynhold H. E. 2002. Landfill Gas: From Rubbish to Resource. Adsorption Research Inc., 9, 87-94.

Kuznicki, S.M., Bell, V.A., Petrovic, I., Blosser, P.W., 1999. Separation of nitrogen from mixtures thereof with methane utilizing barium exchanged ETS-4. US Patent no. 5,989,316.

Kuznicki, S.M., Bell, V.A., Petrovic, I., Bipin, T., 2000. Small-pored crystalline titanium molecular sieve zeolites and their use in gas separation processes. US Patent 6,068,682.

LaCava, A. I.; Koss, V. A.; Wickens, D. 1989. Non-Fickian Adsorption Rate Behaviour of Some Carbon Molecular Sieves. Gas Sep. Purif., 3, 180.

LeVan, M.D., 1998. Adsorption processes and modelling: present and future, Fundamentals of Adsorption (FOA6). F. Meunier , 6, 19-29, Elsevier, Paris.

Li, S.; Martinek, J.G.; Falconer, J.L.; Noble, R.D.; Gardner, T.Q. 2005. High pressure CO_2/CH_4 separation using SAPO-34 membranes. Ind.Chem. Eng. Res., 44, 3220–3228.

Li, S.; Falconer, J. L.; Noble, R. D. 2006. Improved SAPO-34 Membranes for CO_2/CH_4 Separations. Adv. Mater., 18, 2601–2603.

Liu, H.; Ruthven, D. M. 1996. Diffusion in Carbon Molecular Sieves. Proc. Int. Conf. Fundam. Adsorp., M. D. LaVan, ed., Kluwar Press, Boston.

Loughlin, K. F.; Hassan, M. M.; Fatehi, A. I.; Zahur, M. 1993. Rate and Equilibrium Sorption Parameters for Nitrogen and Methane on Carbon Molecular Sieve. Gas Sep. Purif., 7, 264.

Lü,Y.; Doong, S.-J. ; Bülow, M. 2003. Pressure-Swing Adsorption Using Layered Adsorbent Beds with Different Adsorption Properties: I-Results of process simulation, Adsorption, 9,337-347.

Lü,Y.; Doong, S.-J. ; Bülow, M. 2004, Pressure-Swing Adsorption Using Layered Adsorbent Beds with Different Adsorption Properties: II-Experimental Investigation, Adsorption, 10, 267-275.

Marsh, W.D.; Pramuk, F.S.; Hoke, R.C.; Skarstrom, C.W. 1964. Pressure equalization depressurising in heatless adsorption. U.S. Patent No. 3 142 547.

Masahiro, L; Kazuo, H. 1995. Method for Removing Carbon Dioxide from Mixed Gas and Alternative Natural Gas Generating Device Using the Method. World Patent, WO 95526804.

Mitariten, M. 2001. New technology improves nitrogen-removal economics. Oil and Gas Journal, 99, 42-44.

Mitariten, M. 2004. Economic N_2 removal. Hydrocarbon Engineering, 9, 53-57.

Müller, U.; Hesse, M.; Putter, H.; Schubert, M.; Mirsch, D. 2005. Adsorptive Anreicherung von Methan in Methan-haltigen Gasmischen. European Patent EP 1674555.

Nikolic, D.; Giovanoglou, A.; Georgiadis, M. C.; Kikkinides, E. S. 2008. Generic Modeling Framework for Gas Separations Using Multibed Pressure Swing Adsorption Processes, Ind. Eng. Chem. Res., 47, 3156-3169.

Nikolic, D.; Kikkinides, E. S.; Georgiadis, M. C. 2009. Optimization of Multibed Pressure Swing Adsorption Processes, Ind. Eng. Chem. Res., 48, 5388-5398.

Nitta, T.; Shigetomi, T.; Kuro-Oka, M.; Katayama, T. 1984. An adsorption isotherm of multi-site occupancy model for homogeneous surface. J. Chem. Eng. Japan, 17, 39-45.

Online Chemistry Portal: http://www.chemistrylearning.com/adsorption/ (accessed 2011).

Petersson, A., Wellinger, A., 2009. Biogas upgrading technologies –developments and innovations. Brochure of the work in International Energy Agency (IEA) task 37.

Pilarczyk, E.; Knoblauch, K.; Li N.; Strathmann, H. (eds.) 1988. Separation Technology 522, Eng. Foundation, New York.

Pritchard, C. L. 2004. Chasing the Dragon's Tail: Life Cycle Carbon Analysis Applied to CO_2 Sequestration; 7th International Conference on Greenhouse Gas Control Technologies. Vancouver, Canada, September 5-9.

Qinglin, H.; Sundaram, S. M.; Farooq, S. 2003. Revisiting Transport of Gases in the Micropores of Carbon Molecular Sieves. Langmuir, 19, 393-405.

Reid, C. R.; Thomas, K. M. 1999. Adsorption of Gases on a Carbon Molecular Sieves Used for Air Separation: Linear Adsorptives as Probes for Kinetic Selectivity. Langmuir, 15, 3206.

Reid, C. R.; Thomas, K. M. 2001. Adsorption Kinetics and Size Exclusion Properties of Probe Molecules for the Selective Porosity in a Carbon Molecular Sieve Used for Air Separation," J. Phys. Chem. B, 105, 10619.

Ribeiro, A. M.; Grande, C.A.; Lopes, F. V.S.; Loureiro, J.M.; Rodrigues, A.E. 2008 A parametric study of layered bed PSA for hydrogen purification. Chem. Eng. Sci., 63, 5258-5273.

Rutherford, S. W.; Do, D. D. 2000. Adsorption Dynamics of Carbon Dioxide on a Carbon Molecular Sieve 5A. Carbon, 38, 1339.

Ruthven, Douglas M. 1984. Principle of Adsorption and Adsorption Processes. A. Wiley-Interscience Publication.

Ruthven, D. M.; Ragavan, N. S.; Hassan, M. M. 1986. Adsorption and Diffusion of Nitrogen and Oxygen in a Carbon Molecular Sieve. Chem. Eng. Sci., 41, 1325.

Ruthven, D. M. 1992. Diffusion of Nitrogen and Oxygen in Carbon Molecular Sieve. Chem. Eng. Sci., 47, 4305.

Ruthven, D.M.; Farooq, S.; Knaebel, K.S. 1994. Pressure Swing Adsorption; Wiley-VCH, New York.

Ruthven, D. M. 1996. Adsorption: Theory and Practice In: Encontro Brasileiro sobre adsorção, Fortaleza, Anais, 1.

Rynders, R. M.; Rao, M. B.; Sircar, S. 1997. Isotope Exchange Technique for Measurement of Gas Adsorption Equilibria and Kinetics. AIChE J., 43, 2456.

Santos, M.P., Grande, C.A., Rodrigues, A.E. 2010. Reducing heat effects in PSA processes for CO_2 removal. 10th International Conference on Fundamentals of adsorption, Hyogo, Japan.

Santos, M.P.; Grande, C.A.; Rodrigues, A.E. 2011. Pressure Swing Adsorption for Biogas Upgrading. Effect of Recycling Streams in Pressure Swing Adsorption. Ind. Eng. Chem. Res. 50, 974-985.

Schröter, H. J.; Jüntgen, H. 1988. Gas Separation by Pressure Swing Adsorption Using Carbon Molecular Sieves. In: Adsorption: Science and Technology, NATO ASI Series (Rodrigues, LeVan and Tondeur editors), Netherlands: Kluwer Academic Publishers.

Schröter, H. J.; Jüntgen, H.; Rodrigues, A.E.; LeVan, M.D.; Tondeur D. (eds.) 1989. Adsorption: Science and Technology NATO ASI, vol. 158, 269, Kluwer, Dordrecht.

Schröter H. J. 1993. Carbon molecular sieves for gas separation processes. Gas. Sep. Pur., 7, 247-251.

Seery, M. W. 1998. Bulk Separation of Carbon Dioxide from Methane Using Natural Clinoptilolite. World Patent, WO 98/58726.

Shin, H.-C.; Park, J.-W.; Song, H.-C. 2002. Removal characteristics of trace compounds of landfill gas by activated carbon adsorption. Environ. Pollut., 119, 227-236.

Siettos, C. I.; Pantelides, C. C.; Kevrekidis, I. G. 2003. Enabling Dynamic Process Simulators to Perform Alternative Tasks: A Time-Stepper-Based Toolkit for Computer-Aided Analysis, Ind. Eng. Chem. Res., 42, 6795-6801.

Sircar, S.; Koch, W. R. 1986. Adsorptive Separation of Methane and Carbon Dioxide Gas Mixtures. European Patent EP 0193716.

Sircar, S.; Koch, W. R. 1988. Adsorptive Separation of Gas Mixtures. European Patent EP 0257493. **(a)**

Sircar, S.; Kumar, R.; Koch, W. R.; Vansloun, J. 1988. Recovery of Methane from Landfill Gas. United States Patent 4,770,676. **(b)**

Sircar, S. 1995. Influence of Adsorbate Size and Adsorbent Heterogeneity on IAST. AIChe J., 41, 1135-1145.

Sircar, S., 2002. Pressure Swing Adsorption. Ind. Eng. Chem. Res., 41, 1389.

Skarstrom, C.W. 1960. Method and apparatus for fractionating gaseous mixtures by adsorption. U.S. Patent No. 2 944 627.

Srinivasan, R., Auvil, S. R., Schork, J. M., 1995. Mass transfer in carbon molecular sieves - an interpretation of Langmuir kinetics. Chem. Eng. J., 57, 137-144.

Toth, J. 1971. State Equations of the Solid-Gas Interface Layers. Acta Chim. Acad. Sci. Hung., 69, 311-328.

Van den Broeke, L. J. P.; Krishna, R. 1995. Experimental Verification of the Maxwell-Stefan Theory for Micropore Diffusion. Chem. Eng. Sci., 50, 2507.

Voss, C., 2005. Applications of Pressure Swing Adsorption Technology. Adsorption 11,527-529.

Wagner, J.L. 1969. Selective adsorption process. U.S. Patent No. 3 430 418.

Wakao, N. and Funazkri, T. 1978. Effect of fluid dispersion coefficients on particle-to-fluid mass transfer coeficients in packed beds. Chem. Eng. Sci., 33, 1375-1384.

Wang, Q. M.; Shen, D.; Bülow M.; Lau, M. L.; Deng, S.; Fitch, F. R.; Lemcoff, N. O.; Semanscin, J. 2002. Metallo-organic molecular sieve for gas separation and purification. Microporous and Mesoporous Materials., 55, 217-230.

Warmuzinski, K. 2002. Effect of pressure equalization on power requirements in PSA systems. Chem Eng Sci., 57, 1475-1478.

Wasch, A.P.D., Froment, G.F. 1972. Heat transfer in packed beds. Chem. Eng. Sci.,27, 567–576.

Wellinger, A. 2009. Gas upgrading issues. European Biomethane Fuel Conference. Göteborg, Sweden, September 7-9.

Xebec. Biogas purification PSA systems; http://www.xebecinc.com/products-biogas-purification.php (accessed March 2010).

Yang, R. T. 1987. Gas Separation by Adsorption Processes, Butterworth Publishers.

Zupancˇicˇ G.D.; Rosˇ M. 2003. Heat and energy requirements in thermophilic anaerobic sludge digestion. Renewable Energy, 28, 2255-2267.

Appendix

A. Correlations used for estimation of mass and heat transfer parameters employed in the mathematic model

Table A.1. Correlations used for estimation of mass and heat transfer parameters.

Axial mass dispersion (Ruthven et al.,1994)	$\frac{\varepsilon_c D_{ax}}{D_m} = (20 + 0.5ScRe); \quad Re = \frac{\rho_g u d_p}{\mu_g}; \quad Sc = \frac{\mu_g}{\rho_g D_m}$
Axial heat dispersion (Wakao and Funazkri, 1978)	$\frac{\lambda}{k_g} = (7.0 + 0.5PrRe); \quad Pr = \frac{\hat{C}p_g \mu_g}{k_g}$
Molecular diffusion (Bird et al., 2002)	$D_{m,i} = (1 - y_i) / \sum_{\substack{j=1 \\ J \neq i}}^{n} \left(\frac{y_i}{D_{ij}} \right)$
Knudsen diffusion (Ruthven et al.,1994)	$D_{k,i} = 9700 r_p \sqrt{\frac{T_g}{M_w}}$
Film mass transfer (Wakao and Funazkri, 1978)	$Sh = (2.0 + 1.1Re^{0.6} Sc^{1/3}); \quad Sh = \frac{k_f d_p}{D_m}$
Film heat transfer (Wasch and Froment, 1972)	$Nu = (2.0 + 1.1Re^{0.6} Pr^{1/3}); \quad Nu = \frac{h_f d_p}{k_g}$

B. Boundary and initial conditions of the PSA model

Table B.1. Boundary and initial conditions of a PSA process for CO_2/CH_4 separation.

Co-current Pressurization with Feed	
Inlet, $z = 0$	$z = L_c$
$-\frac{\varepsilon D_{ax}}{u(0)}\frac{\partial y(i,0)}{\partial z}\Big\|_{z^+} + y(i,0)\Big\|_{z^+} - y(i,0)\Big\|_{z^-}$	$\frac{\partial y(i,L_c)}{\partial z}\Big\|_{z^-} = 0$
$-\lambda\frac{\partial T_g(0)}{\partial z}\Big\|_{z^+} + uC\tilde{C}_p T_g(0)\Big\|_{z^+} - uC\tilde{C}_p T_g(0)\Big\|_{z^-}$	$\frac{\partial T_g(L_c)}{\partial z}\Big\|_{z^-} = 0$
$P(0) = P_{inlet}$	$u(Lc) = 0$
Feed	
Inlet, $z = 0$	Outlet, $z = L_c$
$-\frac{\varepsilon D_{ax}}{u(0)}\frac{\partial y(i,0)}{\partial z}\Big\|_{z^+} + y(i,0)\Big\|_{z^+} - y(i,0)\Big\|_{z^-}$	$\frac{\partial y(i,L_c)}{\partial z}\Big\|_{z^-} = 0$
$-\lambda\frac{\partial T_g(0)}{\partial z}\Big\|_{z^+} + uC\tilde{C}_p T_g(0)\Big\|_{z^+} - uC\tilde{C}_p T_g(0)\Big\|_{z^-}$	$\frac{\partial T_g(L_c)}{\partial z}\Big\|_{z^-} = 0$
$u(0)C(i,0)\Big\|_{z^+} = u(0)C(i,0)\Big\|_{z^-}$	$P(L_c) = P_{outlet}$
Counter-current Blowdown	
Outlet, $z = 0$	$z = L_c$
$\frac{\partial y(i,0)}{\partial z}\Big\|_{z^+} = 0$	$\frac{\partial y(i,L_c)}{\partial z}\Big\|_{z^-} = 0$
$\frac{\partial \mathrm{T_g}(0)}{\partial z}\Big\|_{z^+} = 0$	$\frac{\partial T_g(L_c)}{\partial z}\Big\|_{z^-} = 0$
$P(0) = P_{low} + (P_E - P_{low})exp(-k_{blow}t)$	$u(L_c) = 0$
Counter-current Purge with methane	
Outlet, $z = 0$	Inlet, $z = L_c$
$\frac{\partial y(i,0)}{\partial z}\Big\|_{z^+} = 0$	$-\frac{\varepsilon D_{ax}}{u(0)}\frac{\partial y(i,L_c)}{\partial z}\Big\|_{z^+} + y(i,L_c)\Big\|_{z^+} - y(i,L_c)\Big\|_{z^-}$
$\frac{\partial T_g(0)}{\partial z}\Big\|_{z^+} = 0$	$-\lambda\frac{\partial T_g(L_c)}{\partial z}\Big\|_{z^+} + uC\tilde{C}_p T_g(L_c)\Big\|_{z^+} - uC\tilde{C}_p T_g(L_c)\Big\|_{z^-}$
$P(0) = P_{outlet}$	$u(L_c)C(i,L_c)\Big\|_{z^+} = u(L_c)C(i,L_c)\Big\|_{z^-}$

Pressure Equalization Depressurization	
$z = 0$	Outlet, $z = L_c$
$\left.\frac{\partial y(i,0)}{\partial z}\right\|_{z^+} = 0$	$\left.\frac{\partial y(i,L_c)}{\partial z}\right\|_{z^-} = 0$
$\left.\frac{\partial T_g(0)}{\partial z}\right\|_{z^+} = 0$	$\left.\frac{\partial T_g(L_c)}{\partial z}\right\|_{z^-} = 0$
$u(0) = 0$	$P(0) = P_E + (P_{low} - P_E)exp(-k_{blow\_eq}t)$

C. Preliminary Studies: 1-Column PSA performance

As already mentioned, in a preliminary study, the behaviour of a PSA process for CH_4/CO_2 separation was studied by making simulations of the performance of one column. These simulations results, described in Table C.1, allow know the most important variables and which are the most sensitive.

Table C.1. 1-Column PSA performance for CH_4/CO_2 separation using zeolite 13X with modified Skarstrom cycle. Depressurization and equalization time last 25 s.

Run	t_{press} (s)	t_{feed} (s)	t_{blow} (s)	t_{purge} (s)	Q_{purge} (SLPM)	P_{high} (bar)	P_{low} (bar)	*L/D*	CH_4 Purity (%)	CH_4 Recovery (%)	CH_4 Productivity ($mol \cdot kg^{-1} \cdot h^{-1}$)	Power ($kW \cdot mol^{-1}$)
3	50	350	200	200	104.16	4.0	0.3	6.75	99.7	70.3	5.4	0.149
4	50	350	200	200	86.8	4.0	0.3	6.75	99.6	74.2	5.7	0.140
5	50	350	200	200	69.44	4.0	0.3	6.75	99.5	78.0	6.0	0.13
6	50	350	200	200	52.08	4.0	0.3	6.75	98.7	81.8	6.3	0.12
7	50	350	200	200	52.08	8.0	0.3	6.75	99.6	76.7	5.9	0.138
8	50	350	200	200	52.08	3.0	0.3	6.75	96.0	82.6	6.3	0.122
9	50	350	200	200	52.08	4.0	0.5	6.75	91.2	82.3	6.3	0.113
10	50	350	200	200	52.08	4.0	0.7	6.75	86.2	82.8	6.3	0.110
11	50	350	200	200	52.08	4.0	0.3	2	99.1	81.8	6.2	0.124
12	50	350	200	200	52.08	4.0	0.3	16	96.3	81.8	6.3	0.124
13	50	375	200	200	52.08	4.0	0.3	6.75	96.5	82.9	6.5	0.116
14	50	330	200	200	52.08	4.0	0.3	6.75	99.3	80.2	6.0	0.133
15	50	350	180	200	52.08	4.0	0.3	6.75	98.8	81.8	6.4	0.125
16	50	350	220	200	52.08	4.0	0.3	6.75	98.8	81.9	6.1	0.123
17	50	350	200	180	52.08	4.0	0.3	6.75	98.0	82.8	6.5	0.123
18	50	350	200	220	52.08	4.0	0.3	6.75	99.3	80.6	5.9	0.120
19	40	350	200	200	52.08	4.0	0.3	6.75	98.8	81.8	6.5	0.121
20	60	350	200	200	52.08	4.0	0.3	6.75	98.8	81.8	6.2	0.124
21	50	350	150	250	52.08	4.0	0.3	6.75	99.5	78.7	6.0	0.130

In this preliminary study, performed with only one column, other important findings are related to the influence of specific variables like feed pressure, purge flowrate and purge step time, blowdown pressure and feed time. As shown in Figure C.1, increasing the purge flowrate results in almost linear drop in product recovery (and unit productivity) without important impacts in CH_4 purity. On the other side, for a constant purge flowrate (see Figure C.2), increasing the purge time has important impact on product purity (from 98 % to 99 %) with losses in recovery of 2 %. Other important variables to be taken into account are the operating pressures (feed and blowdown). Increasing the blowdown pressure to values higher than 0.3 bar resulted in low-purity CH_4 by incomplete desorption of CO_2. Simulations carried out at higher feed pressure resulted in higher purity and lower recovery. The optimal feed pressure should be established from comparison of results at same product purity and overall power consumption.

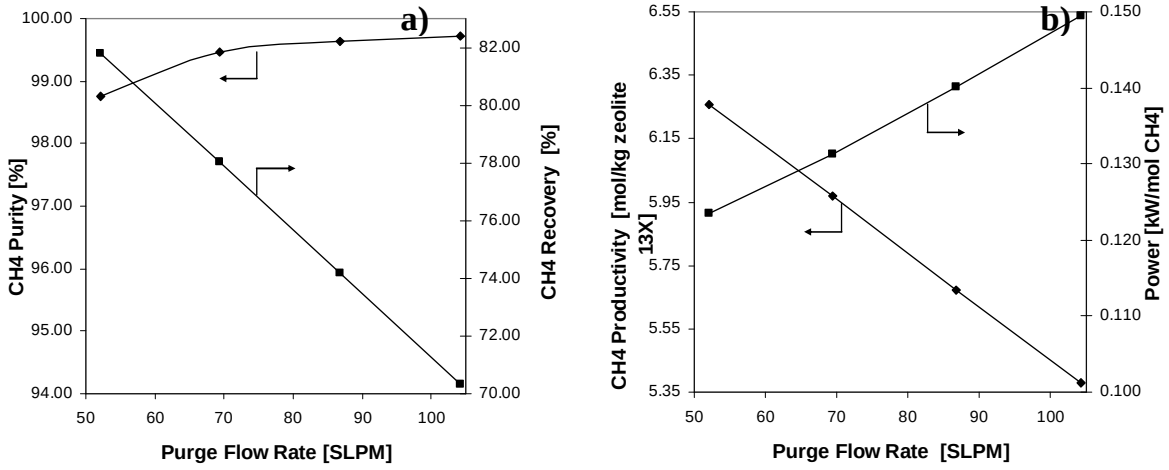

Figure C.1. Effect of purge flowrate in 1-column PSA performance: (a) CH_4 purity and recovery and (b) unit productivity and power consumption.

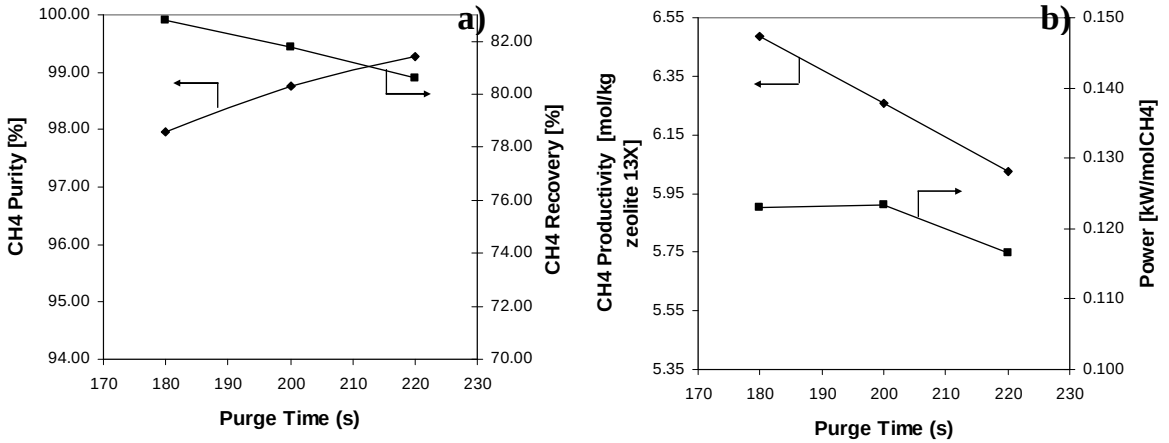

Figure C.2. Effect of purge time in 1-column PSA performance: (a) CH_4 purity and recovery and (b) unit productivity and power consumption.

D. Cycle II: 11-step higher pressure purge step

The cycle presented in Figure 6.1, in Chapter 6, consumes power in the blowdown step and also in the purge step. Another alternative in order to reduce the power consumption of the system is to perform the purge at higher pressure. For this purpose and although not being part of the main objectives of the work, a second cycle configuration, presented in Figure D.1, was also study. In this configuration the purge is performed at higher pressure In this case, the depressurization is divided into two steps and the first portion of gas is used to partially compress the columns after blowdown. With this approach, the purge step can be carried out at higher pressure reducing the overall power consumption.

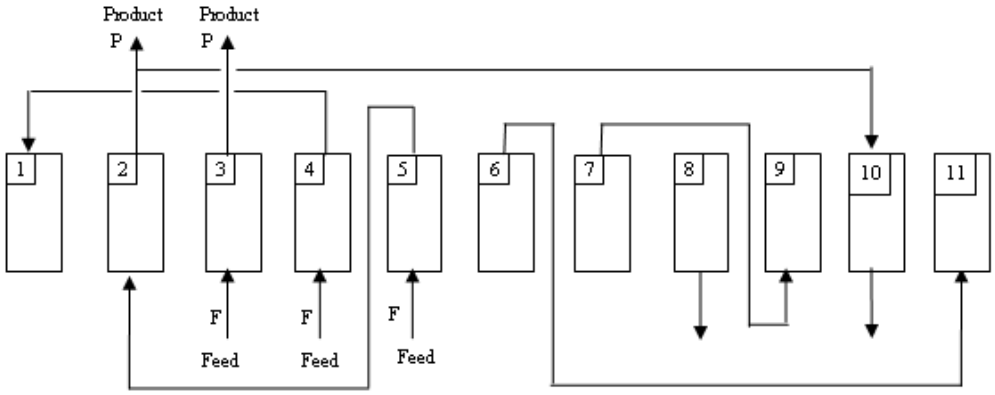

BED	STEPS										
C1	1	2	3	4	5	6	7	8	9	10	11
C2	9	10	11	1	2	3	4	5	6	7	8
C3	7	8		9	10	11	1	2	3	4	5	6
C4	4	5	6	7	8		9	10	11	1	2	3

Figure D.1. PSA cycle scheme used in simulation for PSA Cycle II. Steps are: 1) counter-current product pressurization, 2) trim feed, 3) feed, 4) feed 2, 5) lead adsorption, 6) co-current pressure equalization depressurization 1, 7) co-current pressure equalization depressurization 2, 8) counter-current blowdown, 9) counter-current pressure equalization pressurization 1, 10) counter-current purge with product and 11) co-current pressure equalization pressurization 2.

The second approach studied in this work is a PSA column scheduling such that the purge step is performed at a different pressure than the blowdown step. Using the column array shown in Figure D.1 and CMS-3K, the pressure history of one cycle in cyclic steady state (CSS) is shown in Figure D.2. In fact, using this cycle, it is possible to increase the pressure of the purge and avoid the use of a compressor.

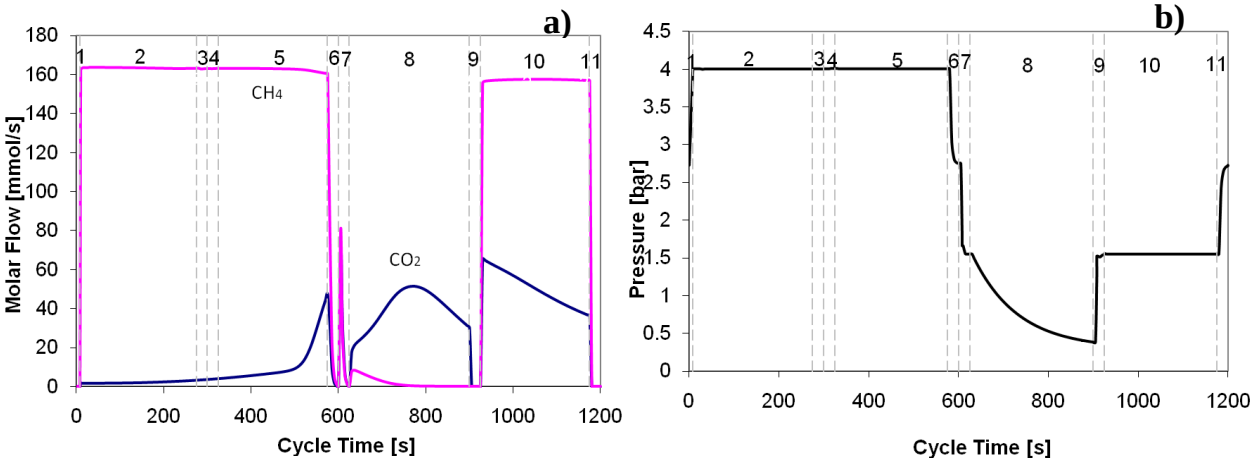

Figure D.2. 4-column simulation of PSA for CH_4-CO_2 separation using CMS-3K. Cycle scheme is shown in Figure D.1 and operating conditions in Table D.1. (Run n). Results presented are: a) molar flowrate of each gas exiting the column and b) and typical pressure history of one CSS cycle used in simulation for PSA Cycle II. Numbers in the figures correspond to the different cycle steps: 1) counter-current product pressurization, 2) trim feed, 3) feed, 4) feed 2, 5) lead adsorption, 6) co-current pressure equalization depressurization 1, 7) co-current pressure equalization depressurization 2, 8) counter-current blowdown, 9) co-current pressure equalization pressurization 1, 10) counter-current purge with product and 11) co-current pressure equalization pressurization 2.

The results for CMS-3K are displayed in Table D.1 while results for zeolite 13X are shown in Table D.2. Even when the purge is performed at a higher pressure, much methane is required to obtain product purity over 98 % and thus the CH_4 recovery is extremely small for both adsorbents. This cycle has resulted in very low unit productivities, product recovery and thus power consumption and will not be considered for further studies.

Table D.1. 4-Column PSA performance for CH_4/CO_2 separation using CMS-3K and the second cycle configuration. All simulations were performed with a feed flowrate of 347.2SLPM and a feed and blowdown pressures of 4 bar and 0.3 bar, respectively. The purge pressure was 1.55 bar. Equalization and feed times were 8 s for the k-o and 25 s for the p-s simulations and the pressurization time was 8 s

Run	t_{trim}	t_{lead}	t_{blow}	t_{purge}	Q_{purge} (SLPM)	CH_4 Purity (%)	CH_4 Recovery (%)	CH_4 Productivity ($mol \cdot kg^{-1} \cdot h^{-1}$)	Total Power ($kW \cdot mol^{-1}$) *	Cycle Power ($kW \cdot mol^{-1}$)
k	200	208	208	200	52.08	93.7	79.3	3.8	0.181	0.0700
l	200	208	208	200	112.84	96.7	55.4	2.6	0.206	0.0986
m	200	208	208	200	156.24	98.2	37.7	1.8	0.247	0.141
n	200	208	208	200	173.6	98.6	30.6	1.5	0.278	0.173
o	200	208	208	200	182.28	98.8	27.0	1.3	0.300	0.195
p	267	275	275	250	130.2	89.0	57.3	2.7	0.153	0.0686
q	267	275	275	250	208.32	98.0	26.8	1.3	0.223	0.143
r	267	275	275	250	234.36	98.7	17.1	0.8	0.305	0.230
s	267	275	275	250	260.4	98.9	7.6	0.4	0.587	0.513

* Total power comprises the cycle power consumption and the power spent in product compression.

Table D.2. 4-Column PSA performance for CH_4/CO_2 separation using zeolite 13X and the second cycle configuration. All simulations were performed with a feed flowrate of 347.2 SLPM and a feed and blowdown pressures of 4 bar and 0.3 bar, respectively. The purge pressure was 1.10 bar. Equalization and feed times were 50 s, pressurization time was 50 s, trim feed and purge times were 200 s, lead and blowdown times were 250 s

Run	Q_{purge} (SLPM)	CH_4 Purity (%)	CH_4 Recovery (%)	CH_4 Productivity ($mol \cdot kg^{-1} \cdot h^{-1}$)	Total Power ($kW \cdot mol^{-1}$) *	Cycle Power ($kW \cdot mol^{-1}$)
t	52.08	87.3	79.9	3.2	0.145	0.0459
u	167.5	98.2	51.6	2.1	0.160	0.0719
v	173.6	98.3	49.8	2.0	0.160	0.0726
w	182.28	98.5	47.3	1.9	0.164	0.0761

* Total power comprises the cycle power consumption and the power spent in product compression.